Am J Physiol Endocrinol Metab 285: E138–E154, 2003.
First published March 18, 2003; 10.1152/ajpendo.00194.2002.

Modeling of Ca^{2+} flux in pancreatic β-cells: role of the plasma membrane and intracellular stores

Leonid E. Fridlyand, Natalia Tamarina, and Louis H. Philipson
Department of Medicine, University of Chicago, Chicago, Illinois 60637

Submitted 6 May 2002; accepted in final form 7 March 2003

Fridlyand, Leonid E., Natalia Tamarina, and Louis H. Philipson. Modeling of Ca^{2+} flux in pancreatic β-cells: role of the plasma membrane and intracellular stores. *Am J Physiol Endocrinol Metab* 285: E138–E154, 2003. First published March 18, 2003; 10.1152/ajpendo.00194.2002.—We have developed a detailed mathematical model of ionic flux in β-cells that includes the most essential channels and pumps in the plasma membrane. This model is coupled to equations describing Ca^{2+}, inositol 1,4,5-trisphosphate (IP_3), ATP, and Na^+ homeostasis, including the uptake and release of Ca^{2+} by the endoplasmic reticulum (ER). In our model, metabolically derived ATP activates inward Ca^{2+} flux by regulation of ATP-sensitive K^+ channels and depolarization of the plasma membrane. Results from the simulations support the hypothesis that intracellular Na^+ and Ca^{2+} in the ER can be the main variables driving both fast (2–7 osc/min) and slow intracellular Ca^{2+} concentration oscillations (0.3–0.9 osc/min) and that the effect of IP_3 on Ca^{2+} leak from the ER contributes to the pattern of slow calcium oscillations. Simulations also show that filling the ER Ca^{2+} stores leads to faster electrical bursting and Ca^{2+} oscillations. Specific Ca^{2+} oscillations in isolated β-cell lines can also be simulated.

Ca^{2+} oscillations; endoplasmic reticulum; pancreatic islets; theoretical model

A RISE in the intracellular free calcium concentration ($[Ca^{2+}]_i$) is a key signal in the initiation of insulin secretion from the pancreatic β-cell. This increase principally results from calcium influx through plasma membrane (PM) Ca^{2+} channels, which open in response to secretagogues, primarily glucose. The metabolism of glucose through glycolysis and the tricarboxylic acid cycle leads to an increase in the cytoplasmic ATP-to-ADP (ATP/ADP) ratio. This causes closure of ATP-sensitive K^+ (K_{ATP}) channels followed by depolarization of the β-cell membrane to the threshold potential where Ca^{2+} channels open, initiating Ca^{2+} influx (4). These events underlie glucose-induced electrical activity that, in pancreatic islets, consists of Ca^{2+}-dependent action potentials.

There is extensive literature describing β-cell electrical activity and its relationship to $[Ca^{2+}]_i$ in intact islets of Langerhans, isolated islet cells, and insulinoma cell lines. Most of the work has been carried out using mouse islets, with some studies using islets from rat, hamster, human, and other species.

Mouse pancreatic β-cells exhibit complex and cyclic spike-burst activity in response to a rise in extracellular glucose concentration. The bursts consist of a depolarized phase of Ca^{2+}-carrying action potentials alternating with a silent phase of repolarization, resulting in oscillations in intracellular Ca^{2+}, which can drive pulses of insulin secretion (28, 37).

The only stimulus required for a complex cyclic spike-burst activity and corresponding $[Ca^{2+}]_i$ oscillations in islets and β-cell clusters is elevation of glucose to levels above 5 and less than ~20 mM. Intermediate glucose concentrations induce two main types of oscillations in mouse pancreatic islets: fast, where the period ranges from 10 to 30 s, and slow, with periods of several minutes (37, 54, 83). Single mouse β-cells can also respond to glucose stimulation with regular oscillations (37).

We have previously studied slow and fast $[Ca^{2+}]_i$ oscillations in islets in response to a variety of conditions (70, 73; unpublished observations). We have also previously reported that a stable, transgenically derived murine insulinoma cell line (βTC3-neo) responds to glucose with slow, large amplitude $[Ca^{2+}]_i$ oscillations but only in the presence of 10–20 mM tetraethylammonium (TEA), a blocker of K^+ channels (74). We have utilized this cell line to characterize glucose-stimulated oscillatory activity (74).

However, the precise interpretation of previous results is limited due to the numerous channels and pumps in β-cells that work concurrently, and identification of physiologically slow variables that drive oscillations remains unclear. To clarify these complex experimental results, we used a mathematical modeling approach. Our goals, then, are twofold: to develop a model for β-cell ion homeostasis, including the bursts and $[Ca^{2+}]_i$ oscillations that can simulate cellular behavior, and to explain on this basis the experimental data for single cells and islets.

Several mathematical approaches in the literature have provided quantitative estimates of glucose-induced insulin secretion with corresponding descriptions of glucose transport, metabolism, and ion regulation (most recent are Refs. 6, 7, 13, 14, 26, 30, 62, 65, and 78). Many phenomena were successfully explained using these models (see DISCUSSION). However, most

Address for reprint requests and other correspondence: L. H. Philipson, Dept. of Medicine, MC 1027, Univ. of Chicago, 5841 S. Maryland Ave, Chicago, IL 60637 (E-mail: L-philipson@uchicago.edu).

The costs of publication of this article were defrayed in part by the payment of page charges. The article must therefore be hereby marked "*advertisement*" in accordance with 18 U.S.C. Section 1734 solely to indicate this fact.

models described one specific phenomenon and therefore included a very restricted set of channels and pumps, so that it is difficult to apply these models to another aim. In addition, newly described experimental results and signaling molecules should be considered.

For this reason, we developed a new model to consider an extended variety of ionic channels and pumps as well as endoplasmic reticulum (ER) calcium sequestration mechanisms that have been identified in β-cells. We simulated whole cell electrical activity and $[Ca^{2+}]_i$, free calcium in the ER ($[Ca^{2+}]_{ER}$), intracellular Na^+ ($[Na^+]_i$), cytosolic ATP ($[ATP]_i$), and inositol 1,4,5-trisphosphate ($[IP_3]_i$) concentrations by use of parameters derived mainly for mouse β-cells. However, in this article, we do not make special consideration of metabolic processes or insulin secretion.

To our knowledge, this article represents the first attempt to include in one model the key ion channels and pumps on both the PM and the ER membrane. Several detailed and comprehensive models have been developed for cardiac muscle and other cell types (67, 71). Here, we employ this approach to investigate the possible role of K^+ channels, Na^+, and IP_3 in regulating β-cell Ca^{2+} oscillations.

MATERIALS AND METHODS

Islet Isolation and $[Ca^{2+}]_i$ Measurement

Isolation of rodent islets. Islets of Langerhans were isolated from the pancreata of 8- to 10-wk-old C57BL/6J mice by collagenase digestion and discontinuous Ficoll gradient methods described previously (85).

Measurement of $[Ca^{2+}]_i$. Islets were loaded with fura 2 for 25 min at 37°C in growth medium (RPMI 1640–10% fetal calf serum, penicillin, and streptomycin) supplemented with 5 mM acetoxymethyl ester of fura 2 (Molecular Probes). $[Ca^{2+}]_i$ was estimated as described elsewhere (74). Dual-wavelength digitized video fluorescent microscopy with fura 2 in single islets was performed using an intensified charge-coupled device (Hammatsu C2400) and Metafluor imaging software (Universal Imaging).

Model Development

Our model of the β-cell combines a parallel conductance membrane model and an inside fluid compartmental model (Fig. 1). The compartmental model describes the time rate of changes in $[Ca^{2+}]_i$, $[Ca^{2+}]_{ER}$, $[Na^+]_i$, and $[ATP]_i$, and $[IP_3]_i$. The extracellular space is assumed to have a relatively large volume, so that ionic concentrations of Ca^{2+}, Na^+, and K^+ there are assumed to be constant.

The corresponding equations for particular channels or pumps that we found in the literature were used even though they were in some cases obtained from cells other than pancreatic β-cells. However, we have considered the origin of the equations employed and their correspondence to biological processes. Model coefficients from the literature were adjusted to simulate the corresponding experimental data as indicated. The basic set of evaluated coefficients is shown in Table 1, denoted as "standard."

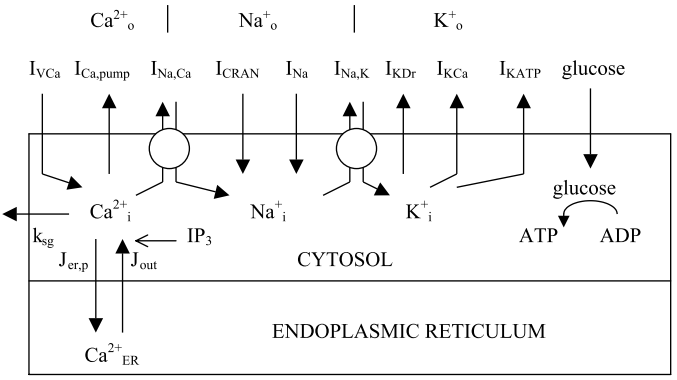

Fig. 1. Schematic representation of currents and ion fluxes through the plasma membrane (PM) and endoplasmic reticulum (ER) membrane that have been included in the whole β-cell model. *Top*: PM currents: I_{VCa}, voltage-dependent Ca^{2+} current; $I_{Ca,pump}$, calcium pump current; $I_{Na,Ca}$, Na^+/Ca^{2+} exchange current; I_{CRAN}, Ca^{2+} release-activated nonselective cation current; I_{Na}, inward Na^+ currents; $I_{Na,K}$, Na/K pump current; I_{KDr}, delayed rectifying K^+ current; I_{KCa}, voltage-independent small-conductance Ca^{2+}-activated K^+ current; I_{KATP}, ATP-sensitive K^+ (K_{ATP}) current; k_{sg}, coefficient of the sequestration rate of intracellular free Ca^+ concentration ($[Ca^{2+}]_i$) by the secretory granules; $J_{er,p}$, uptake of Ca^{2+} by the ER; J_{out}, Ca^{2+} leak current from the ER; IP_3, inositol 1,4,5-trisphosphate.

Plasma membrane currents. The differential equation describing time-dependent changes in the plasma membrane potential (V) is the current balance equation (41)

$$-C_m \frac{dV}{dt} = I_{VCa} + I_{Ca,pump} + I_{Na,Ca} + I_{CRAN} + I_{Na} + I_{Na,K} + I_{KDr} + I_{KCa} + I_{KATP} \quad (1)$$

where C_m is the total membrane capacitance. Model currents include a voltage-dependent Ca^{2+} current (I_{VCa}), a PM calcium pump current ($I_{Ca,pump}$), Na^+/Ca^{2+} exchange current ($I_{Na,Ca}$), Ca^{2+} release-activated nonselective cation current (I_{CRAN}), inward Na^+ currents (I_{Na}), a Na^+/K^+ pump current ($I_{Na,K}$), a delayed rectifier K^+ current (I_{KDr}), voltage-independent small conductance Ca^{2+}-activated K^+ current (I_{KCa}), and the K_{ATP} current (I_{KATP}) (Fig. 1).

Ionic flux across the membrane, J_{xi}, is related to the ionic current by the expression

$$J_{xi} = \frac{I_{xi}}{z_x F} \quad (2)$$

where F and z_x, are Faraday's constant and ionic charge, respectively.

General current equation. The ionic current across channels may be given by the empirical equation (41, p.18)

$$I_{xi} = g_{Xi}(V - V_x) \quad (3)$$

where

$$V_X = \frac{RT}{z_x F} \ln \frac{[X]_o}{[X]_i} \quad (4)$$

$$X = Ca^{2+}, K^+, Na^+ \quad (5)$$

and where g_{Xi} is the whole cell conductance, V_X is the equilibrium potential, R is the universal gas constant, T is absolute temperature, and X_o and X_i are the extra- and intracellular concentrations, respectively.

Table 1. *Standard parameter values*

Current and Parameters	Symbol	Value	Units
I_{VCa}			
Maximum conductance	g_{mVCa}	770	pS
Half-activation potential	V_{Cah}	−19.0	mV
Slope at half-maximum potential	K_{Cah}	9.5	mV
$I_{Ca,pump}$			
Maximum current	P_{mCap}	2,000	fA
Half-maximal pump activity	K_{Cap}	0.1	μM
$I_{Na,Ca}$			
Maximum conductance	g_{NaCa}	271	pS
Ca^{2+} affinity constant	K_{NaCa}	0.75	μM
I_{CRAN}			
Maximum conductance coefficient	g_{mCRAN}	0.7	pS/mV
Reversal potential	V_{CRAN}	0	mV
Half-activation $[Ca^{2+}]_{ER}$ level	K_{Car}	200	μM
I_{Na}			
Maximum conductance	g_{mNa}	1,200	pS
$I_{Na,K}$			
Current coefficient	P_{NaK}	600	fA
I_{KDr}			
Maximum conductance	g'_{mKDr}	3,000	pS
I_{KCa}			
Maximum conductance	g_{mKCa}	130	pS
Affinity constant	K_{KCa}	0.1	μM
I_{KATP}			
Maximum conductance	g'_{mKATP}	24,000	pS
$J_{er,p}$ (SERCA)			
Maximum rate of pumping	P_{CaER}	0.105	μM/ms
Half-maximal pump activity	K_{Carp}	0.5	μM
IP_3 metabolism			
Rate constant of IP_3 production	k_{IP}	0.0003	μM/ms
Rate constant of IP_3 degradation	k_{dIP}	0.00004	ms^{-1}
Half-activation $[Ca^{2+}]_i$	K_{IPCa}	0.4	μM
J_{out}, Ca^{2+}_{ER} leak flux			
Ca^{2+} leak permeability out of the ER	P_{leak}	0.0001	pl/ms
Ca^{2+}_{ER} maximum permeability through open IP_3-activated channels	P_{IP3}	0.0012	pl/ms
Affinity constant of $[Ca^{2+}]_i$ to IP_3R	K_{RCa}	0.077	μM
Affinity constant of $[IP_3]_i$ to IP_3R	K_{IP3}	3.2	μM
Coefficient of the Ca^{2+} sequestration rate	k_{sg}	0.0001	ms^{-1}
ATP homeostasis			
Concentration of intracellular nucleotides	$[A]_o$	4,000	μM
Rate constant of ATP production	k_{ADP}	adjusted	ms^{-1}
Rate constant of Ca^{2+}-dependent ATP consumption	$k_{ATP,Ca}$	0.00005	$\mu M^{-1}ms^{-1}$
Rate constant of permanent ATP consumption	k_{ATP}	0.00005	ms^{-1}

CRAN, Ca^{2+} release-activated nonselective cation; SERCA, sarco-(endo)plasmic reticulum Ca^{2+}-ATPase; IP_3, inositol 1,4,5-triphosphate; ER, endoplasmic reticulum; IP_3R, IP_3 receptor. For other definitions and explanations see text.

Whole cell conductance may depend on ion concentrations and voltage. These dependencies will be specified for each conductance as they are discussed.

I_{VCa}. The whole cell Ca^{2+} current in mouse β-cells flows principally through voltage-activated Ca^{2+} channels (29, 80). This current increases when the membrane is depolarized. *Equation 3* was used for this current. The current/voltage relationship of this current $[p_{VCa}(V)]$ can be described by a Boltzmann-type activation curve (7, 9). Then

$$I_{VCa} = g_{mVCa} p_{VCa}(V)(V - V_{Ca}) \quad (6)$$

where

$$p_{VCa}(V) = \frac{1}{1 + \exp[(V_{Cah} - V)/K_{Cah}]} \quad (7)$$

and where g_{mVCa} is the maximum whole cell conductance, V_{Cah} is the half-activation potential, and K_{Cah} is the slope at half-maximal potential.

At physiological Ca^{2+} concentrations, the measured V_{Cah} varies from −3.8 mV (80) and −16.7 mV (45) to −19 mV (9), and K_{Cah} extends from 6.6 mV (45) and 8.4 mV (80) to 13 mV (9). In our model, these coefficients were fitted to be inside these regions (Table 1).

According to Göpel et al. (33) the mean integrated Ca^{2+} current observed during a 100-ms depolarization to −20 mV in the β-cell in situ was 7.7 pC at $[Ca^{2+}]_o$ = 2.6 mM. This result can be obtained from *Eq. 6* of our model, with g_{mVCa} = 995 pS and $[Ca^{2+}]_i$ = 0.05 μM. We set g_{mVCa} = 770 pS as the standard condition for our model (Table 1). This value is close to that estimated above. The current/voltage relationship calculated using *Eq. 6* is in good correlation with data for β-cells in situ (33).

PM Ca^{2+} pumps ($I_{Ca,pump}$). PM Ca^{2+} pumps are now well recognized as a primary system for the specific expulsion of Ca^{2+} from β-cells (87). However, their kinetic properties are not well studied in these cells. For this reason, the general properties of PM Ca^{2+} pumps were used for the calculations.

It is now generally established that the Ca^{2+}/ATP stoichiometry of the PM Ca^{2+} pump is 1 (10, 66) and that the reconstituted PM pumps are capable of establishing a membrane potential while operating with H^+/Ca^{2+} = 1 (40). PM and ER Ca^{2+} pumps do not have the sensitivity to ATP at the millimolar ATP concentrations that exist in physiological conditions (10). The K_m is <0.5 μM Ca^{2+} for activated PM pumps (10, 66). On the basis of these data, the Ca^{2+} current through PM Ca^{2+} pumps was expressed in our model as (see 62)

$$I_{Ca,pump} = P_{mCap} \frac{[Ca^{2+}]_i^2}{K_{Cap}^2 + [Ca^{2+}]_i^2} \quad (8)$$

where P_{mCap} is a maximum current and K_{Cap} is the value for the half-activation calcium concentration. K_{Cap} was set to 0.1 μM, which is within the range of experimental observations for other preparations. P_{mCap} (Table 1) is correspondingly above the evaluated lower limit (830 fA) that we obtained (see RESULTS).

Na^+/Ca^{2+} exchanger ($I_{Na,Ca}$). The lack of specific inhibitors hinders the experimental assessment of the role of the Na^+/Ca^{2+} exchanger. However, a detailed investigation of the β-cell electrogenic 3 Na^+/Ca^{2+} exchanger was recently reported (25), and the exchanger current ($I_{Na,Ca}$) was taken as follows from this work

$$I_{Na,Ca} = g_{NaCa} \frac{[Ca^{2+}]_i^5}{[Ca^{2+}]_i^5 + K_{NaCa}^5} (V - V_{Na,Ca}) \quad (9)$$

where

$$V_{Na,Ca} = \frac{RT}{F} \left(3 \ln \frac{[Na^+]_o}{[Na^+]_i} - \ln \frac{[Ca^{2+}]_o}{[Ca^{2+}]_i} \right) \quad (10)$$

and where g_{NaCa} is the maximum whole cell conductance, and K_{NaCa} is affinity constant.

One can calculate from Gall et al. (25) that g_{NaCa} = 271 pS (as $C_m \cdot \check{g}_{Na/Ca}$ from their *Eq. 2*), and we used this value for g_{NaCa} in our model.

Similarly, those authors found K_{NaCa} to be 1.5 μM (25). However, an insignificant $I_{Na,Ca}$ and a correspondingly very

small influence of the Na^+/Ca^{2+} exchanger on the model solutions were obtained at $K_{NaCa} = 1.5$ μM. This result does not correspond to the data involving the effect of this exchanger on glucose-induced electrical activity in intact pancreatic islets (25). This apparent contradiction is probably due to the use of low ATP concentration in the perforated patch whole cell experiments in Ref. 25; therefore, K_{NaCa} (1.5 μM) should only be considered as an upper limit. Data from different cell types show that ATP induces a dramatic increase in the intracellular Ca^{2+} affinity for the Na^+/Ca^{2+} exchanger (20). Correspondingly, a lower value for K_{NaCa} (0.75 μM) was employed in our model to fit glucose-induced β-cell oscillation patterns at an increased ATP content.

I_{CRAN}. I_{CRAN} is a nonselective cation current whose conductance is regulated by the ER Ca^{2+} content. In mouse β-cells, it could be activated either indirectly by ER Ca^{2+} store depletion or directly by maitotoxin (84, 88, 89). However, the mechanism for coupling ER Ca^{2+} store depletion with CRAN remains an unresolved question.

In our model, only Na^+ can penetrate into the cell via this channel, reflecting experimental results under physiological concentrations of cations (52, 84, 88). The current/voltage relationship of this current [$p_{CRAN}(V)$] was roughly linear, with a reversal potential close to 0 mV (52, 84, 88). In previous models, it was suggested that the regulation of I_{CRAN} depends on $[Ca^{2+}]_{ER}$ (8, 14, 62). We take this dependence following Ref. 62. *Equation 3* can be written for this Na^+ inward current

$$I_{CRAN} = f_{CRAN} p_{CRAN}(V)(V - V_{Na}) \quad (11)$$

where

$$f_{CRAN} = \frac{-g_{mCRAN}}{1 + \exp\{([Ca^{2+}]_{ER} - K_{Car})/3\}} \quad (12)$$

$$p_{CRAN}(V) = V - V_{CRAN} \quad (13)$$

and g_{mCRAN} is the maximum whole cell conductance, f_{CRAN} is the voltage-independent part of the current, K_{Car} is the half-activation $[Ca^{2+}]_{ER}$ level, and V_{CRAN} is the reversal potential.

K_{Car} has been modified in our model, and it is now 200 rather than 40 μM (as accepted in Ref. 62), because the $[Ca^{2+}]_{ER}$ is usually found to be in the hundred micromolar range (see Ref. 86).

I_{Na}. The general equation for I_{Na} is derived from *Eq. 3*. The relationship between conditioning voltage and relative current amplitude for tetrodotoxin-blockable component of the I_{Na} [$p_{Na}(V)$] was characterized (33) as the Boltzmann equation. Then

$$I_{Na} = g_{mNa} p_{Na}(V)(V - V_{Na}) \quad (14)$$

where

$$p_{Na}(V) = \frac{1}{1 + \exp[(104 + V)/8]} \quad (15)$$

The maximum value of whole cell conductance (g_{mNa}) was evaluated from the data (33), where it was found that $I_{Na} = -392$ pA at $V = -140$ mV. This I_{Na} value can be obtained from *Eq. 14,* with g_{mNa} as 1,200 pS when $[Na^+]_i$ is close to 0 and $[Na^+]_o = 140$ mM. (We used $[Na^+]_i = 0.1$ mM for this calculation). This value was used for standard conditions (Table 1).

Na^+-K^+ active transport ($I_{Na,K}$). Electrogenic Na^+-K^+-ATPase extrudes three Na^+ ions in exchange for two K^+ ions for each molecule of ATP hydrolyzed, generating a net outward flow of cations through the β-cell PM (68). However, its kinetic properties have not been studied in β-cells. For this reason, we employed the general model (12) as was done previously for β-cells (65) (see APPENDIX A).

I_{KDr}. The principal type of voltage-dependent K^+ current in β-cells is the I_{KDr}. Kv2.1 is a likely candidate for the principal delayed rectifier isoform expressed in β-cells (56, 70).

Equation 3 was used; however, the formulation (26, 78) is employed for whole cell conductance.

$$I_{KDr} = g'_{mKDr} n(V - V_K) \quad (16)$$

where g'_{mKDr} is the maximal whole cell conductance, and n is the general gating variable, which is determined in APPENDIX B.

The value of g'_{mKDr} (*Eq. 16*) is calculated to be 3,000 pS for standard conditions. This is comparable to the value used in Refs. 8, 26, and 65.

Family of KCa channels (I_{KCa}). The voltage-independent small-conductance Ca^{2+}-activated K^+ channels (SK channels) are also expressed in β-cells (unpublished observations). It is quite plausible that these channels play an important role in $[Ca^{2+}]_i$ oscillations (32).

Equation 3 was used for this channel. Ca^{2+} activates I_{KCa} currents [$f(Ca^{2+})$] in a sigmoidal fashion (49, 53). However, there are no data on the exact dependence in β-cells. The Hill equation was used to model this relationship, where the Hill coefficient equals 3 (14) or 5 (62). We also use a Hill equation, but with a Hill coefficient equal to 4

$$I_{KCa} = g_{mKCa} f(Ca^{2+})(V - V_K) \quad (17)$$

where

$$f(Ca^{2+}) = \frac{[Ca^{2+}]_i^4}{[Ca^{2+}]_i^4 + K_{KCa}^4} \quad (18)$$

and K_{KCa} is affinity constant.

K_{KCa} varies in the 0.05–0.9 μM range (Ref. 41, p. 144). However, SK3 channels may be the predominant SK family member in β-cells (unpublished observations), and because $K_{KCa} = 0.1$ μM was found for SK3 channels by Carignani et al. (11), this value was used in our model.

It is unlikely that the large-conductance Ca^{2+}-activated K^+ channel (BK channel) encoded by the *slo* gene plays an important role in the generation of oscillatory activity in β-cells (50), although several previous models of β-cell bursting have included this channel (78). We therefore did not include it in our considerations.

K_{ATP} channels (I_{KATP}). Equation 3 was used for this channel. However, we adopt here a kinetic model for the value of whole cell conductance (see Refs. 43, 58, 65). Then

$$I_{KATP} = g'_{mKATP} O_{KATP}(V - V_K) \quad (19)$$

where g'_{mKATP} is the maximal value of the whole cell conductance, and O_{KATP} is the fraction of channels open, which is considered in APPENDIX C.

The value g'_{mKATP} was evaluated to be 24 nS for the standard coefficient, which is comparable to the value used in Refs. 59 and 65. Then it can be calculated from *Eqs. 19* and *C1* (APPENDIX C) that the value of the whole cell conductance ($g'_{mKATP}\ O_{KATP}$) is 0.94 nS at $[ATP]_i = 0$. This value falls in the range between 0.2 and 3.0 nS that was measured for the maximum K_{ATP} conductance reported for single mouse β-cells (48).

Fluid Compartmental Model

The material balance equation for calcium depends on three processes: entry, extrusion, and buffering (Fig. 1).

Calcium enters the β-cells primarily through voltage-activated Ca^{2+} channels by diffusion along an inwardly directed electrochemical gradient (I_{VCa}). The maintenance of this ionic gradient depends on a Ca^{2+}-extruding mechanism in the PM and Ca^{2+} sequestration by intracellular organelles. At the PM, three processes are involved in transporting Ca^{2+} out of the cell: a Ca^{2+} pump, a Na^+/Ca^{2+} exchanger, and removal of Ca^{2+} sequestrated in insulin granules by exocytosis. In addition, both the ER and mitochondria can accumulate Ca^{2+} via pumps. Even though Ca^{2+} is critical for mitochondrial function, for the present we do not include mitochondrial Ca^{2+} stores, since it appears that both the volume of mitochondria and its Ca^{2+} concentration are small relative to the ER (2, 18).

Sarco(endo)plasmic reticulum Ca^{2+}-ATPase pump. Uptake of Ca^{2+} into the ER is mediated in β-cells by sarco(endo)plasmic reticulum Ca^{2+}-ATPases (SERCAs) with an unusually low value for the half-activation calcium concentration (≤0.4 μM) (27). The Ca^{2+}/ATP stoichiometry of the SERCA is 2 (10, 66). The equation for SERCA was written in the same form as the Ca^{2+} PM pump (*Eq. 8*; see also Ref. 62)

$$J_{er,p} = P_{CaER}\frac{[Ca^{2+}]_i^2}{[Ca^{2+}]_i^2 + K_{Carp}^2} \quad (20)$$

where $J_{er,p}$ is the flux into the ER through SERCA pumps per cytosol volume, K_{Carp} is the half-maximal pump activity, and P_{CaER} is the maximum rate of pumping. The lower limit for this parameter was evaluated (see RESULTS) as $P_{CaER} = 0.026$ μM/ms for the data from Ref. 25. The evaluated parameter for standard conditions (Table 1) is correspondingly above this lower limit. K_{Carp} was taken as 0.5 μM, a value close to experimental data (27).

IP_3 metabolism. In the pancreatic β-cell, there is clear evidence that IP_3 is an important cellular messenger inducing Ca^{2+} mobilization from intracellular stores by binding to specific receptors located on intracellular Ca^{2+} stores and is the main calcium release channel from the ER in β-cell tissues (38). However, we could not find any mathematical models of β-cell regulation that used IP_3 as an independent variable.

Different mechanisms seem to be available in the β-cells for stimulating IP_3 production; however, only the modulation of inositol lipid-specific phospholipase activity by changes in Ca^{2+} is well studied (3). For this reason, the $[Ca^{2+}]_i$ dependence was only modeled as the Hill function with a Hill coefficient of 2 (3).

The subsequent kinetics of IP_3 in β-cells is unknown. Therefore, we assume simply that IP_3 is converted to inactive metabolites at a rate proportional to its concentration. Then synthesis and degradation of IP_3 are described by the equation

$$\frac{d[IP_3]_i}{dt} = k_{IP}\frac{[Ca^{2+}]_i^2}{[Ca^{2+}]_i^2 + K_{IPCa}^2} - k_{dIP}[IP_3]_i \quad (21)$$

where k_{IP} is the rate constant of IP_3 production, k_{dIP} is the rate constant of IP_3 degradation, and K_{IPCa} is the half-activation of the IP_3 production by calcium concentration.

The time constants k_{IP} and k_{dIP} (Table 1) were picked to correctly reproduce the experimentally observed time course of the average $[Ca^{2+}]_i$ during the slow $[Ca^{2+}]_i$ oscillations (see RESULTS). K_{IPCa} is taken as 0.4 μM (36). The fitted parameter k_{dIP} (0.04 s^{-1}, Table 1; half-life is 17.3 s) is inside the region of a half-life from 1 to 30 s that has been found for different cells with a radius of ~5 μm and above (79), similar to that of β-cells.

Ca^{2+}_{ER} mobilization. A Ca^{2+} leak current (J_{out}) from the ER per whole cell was taken according to Mears et al. (62)

$$J_{out} = (P_{leak} + P_{IP3}O_\infty)([Ca^{2+}]_{ER} - [Ca^{2+}]_i) \quad (22)$$

where P_{leak} is the Ca^{2+} leak permeability out of the ER, P_{IP3} is the maximum permeability through open IP_3-activated channels, and O_∞ is the fraction of open IP_3-activated Ca^{2+} channels.

The type III IP_3 receptor (IP_3R) is the main calcium release channel in the β-cell ER (38). Apparently, in normal physiological conditions, the O_∞ does not depend on the change of ATP concentration (57). The initial dependence of the IP_3R maximum open probability vs. cytosolic Ca^{2+} could be well fitted to a Michaelis-Menten-type saturating equation with an affinity of 0.077 μM for $[Ca^{2+}]_i$ (60).

However, there are conflicting data concerning IP_3 action. According to Hagar and Ehrlich (39), the Hill equation with a Hill coefficient close to 2 was found for the effect of IP_3 on O_∞ in vitro. On the other hand, the Hill number for low degrees of saturation of the IP_3R was estimated at ~3.5 in vivo for rat basophilic leukemia cells (63). On the basis of these data, the Hill coefficient is set equal to 3. Then

$$O_\infty = \frac{[Ca^{2+}]_i}{[Ca^{2+}]_i + K_{RCa}}\frac{[IP_3]_i^3}{[IP_3]_i^3 + K_{IP3}^3} \quad (23)$$

where K_{RCa} is the affinity constant of the $[Ca^{2+}]_i$ to IP_3R, and K_{IP3} is the constant for IP_3 binding to a channel. K_{IP3} is 3.2 μM (39).

Ca^{2+} and Na^+ dynamics. The cytosolic and ER calcium concentrations and Na^+ cytosolic concentration are determined by the ion fluxes across the plasma and ER membranes. However, calcium concentrations are strongly buffered in cells (77). This can be modeled using special coefficients for the fraction of free Ca^{2+} in the cytoplasm and ER (14, 62, 71). The Ca^{2+} leak from cells by β-granule exocytosis was modeled previously (14) as a rate proportional to $[Ca^{2+}]_i$. We employed a similar approach.

On the basis of the foregoing consideration, the equations for Ca^{2+} and Na^+ concentrations can be written as

$$\frac{d[Ca^{2+}]_i}{dt} = f_i\left(\frac{-I_{VCa} + 2I_{Na,Ca} - 2I_{Ca,pump}}{2FV_i} - J_{er,p} + \frac{J_{out}}{V_i}\right) - k_{sg}[Ca^{2+}]_i \quad (24)$$

$$\frac{d[Ca^{2+}]_{ER}}{dt} = \frac{f_{er}}{V_{er}}(J_{er,p}V_i - J_{out}) \quad (25)$$

$$\frac{d[Na^+]_i}{dt} = \frac{-3I_{Na,Ca} - 3I_{Na,K} - I_{Na} - I_{CRAN}}{V_iF} \quad (26)$$

where f_i and f_{er} are the fractions of free Ca^{2+} in cytoplasm and ER, V_{er} and V_i are the effective volumes of the ER and cytosolic compartments, and k_{sg} is a coefficient of the sequestration rate of $Ca^{2+}{}_i$ by the secretory granules.

It has been proposed that the Ca^{2+}-binding capacity inside the ER is lower than in the cytoplasm (69). This can increase the fraction of free Ca^{2+} in ER; therefore, we used a value of f_{er} threefold higher than f_i (Table 2).

ATP homeostasis. ATP concentration in the cytosol increases somewhat with an increase in glucose supply (2). However, the rate of ATP production and utilization is a complex function of the concentrations of ATP_i, ADP_i, Ca^{2+}, glucose, and numerous other factors. For simplicity, we have chosen a first-order reaction to express the rate of ATP_i production from ADP_i.

Table 2. *Cell and external parameters*

Parameters	Symbol	Value	Units	Reference
Cytosol volume	V_i	0.764	pL	(16)
ER volume	V_{er}	0.280	pL	(16)
Total membrane capacitance	C_m	6158	fF	(62)
Fraction of free Ca^{2+} in cytoplasm	f_i	0.01		(58)
Fraction of free Ca^{2+} in ER	f_{er}	0.03		Adjusted
Intracellular K^+ concentration	$[K^+]_i$	132.4	mM	Adjusted*
Extracellular K^+ concentration	$[K^+]_o$	8	mM	Adjusted
Extracellular free Ca^{2+} concentration	$[Ca^{2+}]_o$	2.6	mM	(58)
Extracellular Na^+ concentration	$[Na^+]_o$	140	mM	Adjusted
Thermal voltage, RT/F (37°C)		26.73	mV	(41)

*Intracellular $[K^+]_i$ and extracellular K^+ concentrations $[K^+]_o$ were adjusted to give an equilibrium potential (*Eq. 4*) of −75 mV.

Clearly, there is some basal level of ATP_i consumption in a cell at low glucose and $[Ca^{2+}]_i$. There is also ATP consumption by the PM and ER Ca^{2+} pumps and by the electrogenic Na^+-K^+-ATPase in our model. However, there is considerable evidence that other ATP consumption processes are accelerated by an increase in $[Ca^{2+}]_i$ in β-cells (2, 23, 76). For this reason, an additional term for ATP consumption was introduced, which depends on an increase in $[Ca^{2+}]_i$. Then

$$\frac{d[ATP]_i}{dt} = k_{ADP}[ADP]_i - \frac{I_{Na,K} + I_{Ca,pump}}{V_i F} - \frac{J_{er,p}}{2} - (k_{ATP,Ca}[Ca^{2+}]_i + k_{ATP})[ATP]_i \quad (27)$$

where

$$[ATP]_i + [ADP]_i = [A]_o \quad (28)$$

k_{ADP} is the rate constant of ATP_i production, $k_{ATP,Ca}$ is the rate constant of ATP_i consumption that accelerates as $[Ca^{2+}]_i$ increases, and k_{ATP} is the permanent rate constant of ATP_i consumption.

The general concentration of intracellular nucleotides ($[A]_o$) was assumed to be constant. The measured concentration of adenine nucleotides in pancreatic islets varies within the limits of 2–10 mM (23). We have taken $[A]_o$ to be inside this range (4 mM).

It is important to find a range of parameters for ATP dynamics. According to the calculations in Ref. 23, the rate of ATP_i production in β-cells may run to ~0.5 μmol $ATP \cdot s^{-1} \cdot g$ dry wt^{-1} at low glucose concentrations and 1 μmol $ATP \cdot s^{-1} \cdot g$ dry wt^{-1} at high glucose concentrations. Matschinsky et al. (61) found the corresponding level of adenine nucleotides to be ~20 μmol/g dry wt. Then the mean rate of ATP_i production per second can be estimated roughly as a part of the general quantity of intracellular nucleotides per unit of volume, that is, as 0.025 or 0.05 $[A_o]$/s (or 0.1 and 0.2 mM/s) at low and high glucose concentrations, respectively.

The constants $k_{ATP,Ca}$ and k_{ATP} (*Eq. 27* and Table 1) were fitted to simulate both the observed pattern of $[Ca^{2+}]_i$ oscillations and the evaluated rate of ATP_i production in β-cells above. The simulation of low glucose concentration (k_{ADP} = 0.03 s^{-1}) leads in our model to a steady-state $[ADP]_i$ of 3.068 mM (Table 3) and to a corresponding rate of ATP_i production (k_{ADP} $[ADP]_i$) of 0.092 mM/s. The simulation of slow $[Ca^{2+}]_i$ oscillations at high glucose levels (k_{ADP} = 0.37 s^{-1}; Fig. 3) yields a mean $[ADP]_i$ of 0.7 mM and to the rate of ATP_i production as 0.26 mM/s. This correlates well with the values evaluated above.

Computational aspects. The spread of current between electrically coupled β-cells most probably contributes to the synchronization of the electrical activity and $[Ca^{2+}]_i$ oscillations throughout an islet (33, 37). For this reason, we consider islets as an assemblage of cells with similar properties and perform the computer simulation only for some mean individual cell.

The complete system consists of seven state variables: differential equations describing the time rate of change in PM potential (V), Ca^{2+}, Na^+, ATP, and IP_3 concentrations in cytoplasm, calcium concentration in ER, and the differential equations characterizing the voltage-dependent gating variable (n) for the delayed rectifier K^+ channels (*Eqs. 1, 21, 24–27, B1*). The units used in the model are time in milliseconds (ms), voltage in millivolts (mV), current in femtoamperes (fA), concentration in micromoles per liter (μM), conductance in picosiemens (pS), capacitance in femtofarads (fF), and temperature in degrees Kelvin (°K).

The model and cell parameters are given in Tables 1–3. These tables and the appendixes contain all the information necessary to carry out the simulations presented in this paper. However, the rate constant for ATP_i production (k_{ADP}) is represented in every figure legend.

Simulations were performed by forward integration of the coupled system of differential equations. We used two integrated software environments: "Content" for the IBM-compatible personal computer using an implicit fourth-order Runge-Kutta or Rodau IIA method (15) and "Virtual Cell" accessible via the Internet (55).

This model is available for direct simulation on the website "Virtual Cell" (www.nrcam.uchc.edu) in "MathModel Database" on the "math workspace" in the library "Fridlyand" with the name "Chicago.1".

RESULTS

Validation of the Model

It was possible to evaluate the values of the rates of Ca^{2+} pumps from the simulation of the data from Ref. 25, where the $[Ca^{2+}]_i$ transients were induced by a 2-s depolarization. Gall et al. (25) found that the time constant for the decrease in $[Ca^{2+}]_i$ is ~1.8 s when Ca^{2+}-ATP pumps on the PM and ER were activated and 4.6 s when Ca^{2+}-ATP pumps on the ER were inhibited by thapsigargin (Tg). This was determined under conditions where the Na^+/Ca^{2+} exchanger was inactive, i.e., $g_{NaCa} = 0$, granule exocytosis was lacking ($k_{sg} = 0$), and IP_3R was closed ($P_{IP3} = 0$). Using *Eqs. 9* and *21,* we found that these data can be well simulated at P_{CaER} = 0.026 μM/ms and P_{mCap} = 830 fA. However,

Table 3. *PM potential and intracellular ion concentrations at steady state at the simulation of low glucose concentration (k_{ADP} = 0.03 s^{-1})*

Symbol	Value	Units
V	−60.9	mV
$[Ca^{2+}]_i$	0.085	μM
$[Ca^{2+}]_{ER}$	22.8	μM
$[IP_3]_i$	0.33	μM
$[ATP]_i$	932.1	μM
$[Na^+]_i$	9858	μM
n	0.00123	

PM, plasma membrane.

these values should be considered as a lower limit, whereas the experiments in Ref. 25 were made in conditions of low ATP concentration, and it is probable that Ca^{2+} pumps were in an inactivated form. Correspondingly, higher values were fitted in our model (see Table 1).

A number of parameters were taken from the literature, such as channel and pump kinetics (see MATERIALS AND METHODS). However, because these values were sometimes derived from experiments with different cell lines and specific experimental conditions, these parameters were constrained to be within a range consistent with our own system. Other parameters were fitted to simulate the pattern of fast and slow bursting of electrical activity and $[Ca^{2+}]_i$ oscillations in β-cells. The parameters that yield these oscillations are the standard values given in Table 1. A computer simulation at a low ATP production rate and the coefficients from Tables 1 and 2 were used to obtain the steady-state data corresponding to low glucose concentrations (Table 3).

Islet Simulations

Slow Ca^{2+} oscillations. Slow Ca^{2+} oscillations occur spontaneously during glucose stimulation (Fig. 2). They are characterized by a descending phase in two components. A rapid decrease in $[Ca^{2+}]_i$ is followed by a slower phase. Similar data were obtained by many investigators for slow oscillations (27, 37, 64). It was also shown that a rapid decrease in $[Ca^{2+}]_i$ coincided with the closure of voltage-dependent Ca^{2+} channels (27).

A typical computer simulation of slow oscillations with the patterns of membrane potential and corresponding concentrations is illustrated in Fig. 3, *left*. It was obtained by introducing a step increase in the rate constant of ATP_i production from the resting conditions (Table 3) to an intermediate value. A detailed pattern of the concentration changes and corresponding currents is shown in Fig. 5*A* for a single oscillation.

As can be seen in Fig. 3, the acceleration of ATP_i production increases the $[ATP]_i/[ADP]_i$ ratio after a step increase of k_{ADP}. This closes K_{ATP} channels in the PM. This closure decreases the I_{KATP} that depolarizes the PM, leading to the opening of voltage-dependent Ca^{2+} channels, the stimulation of Ca^{2+} influx, and, eventually, a rise in $[Ca^{2+}]_i$. Increasing the I_{VCa} makes a contribution to depolarization of the PM by itself. The beginning of electrical spiking is generated at threshold PM potential to form bursts and leads to $[Ca^{2+}]_i$ increase (Fig. 3*B*, *arrow 1*). Continuous spiking follows up to a point at which the repolarizing processes lead to decreased PM potential. This in turn leads to the closure of voltage-gated Ca^{2+} channels and the continuous spiking terminates (Fig. 3*B*, *arrow 2*). In the silent phase, slow depolarization of the PM begins until all processes repeat, leading to continuous oscillations.

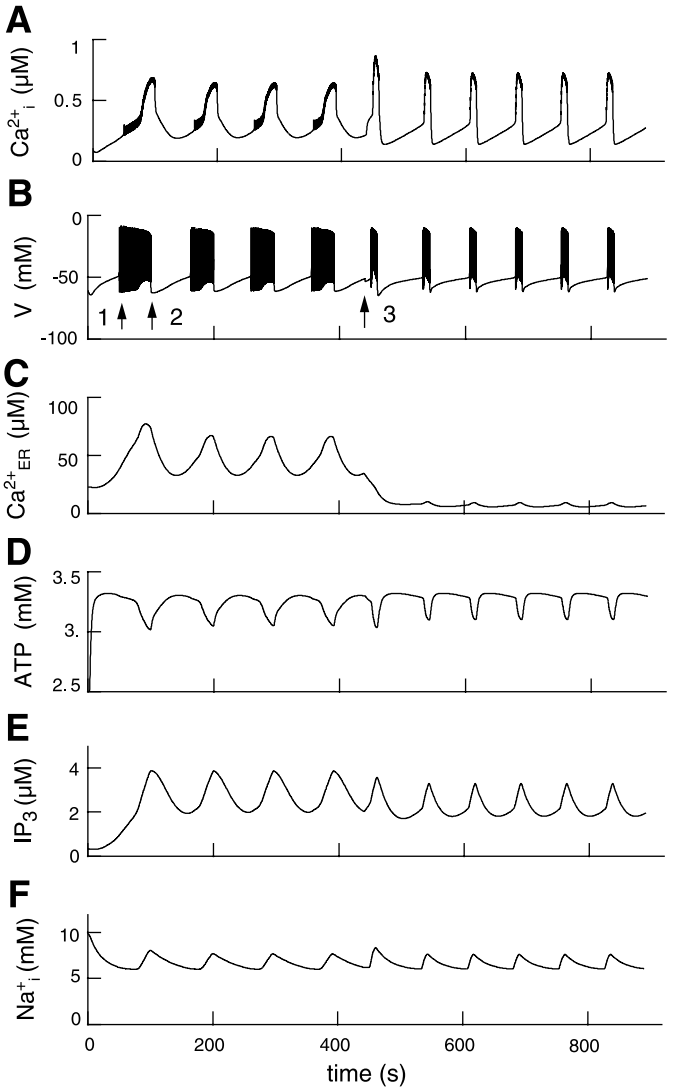

Fig. 3. Glucose-induced slow electrical bursting and $[Ca^{2+}]_i$ oscillations were simulated at a step increase of the rate constant of ATP_i production from a low to an intermediate value (from $k_{ADP} = 0.03\ s^{-1}$ to $0.37\ s^{-1}$) at $t = 0$ at initial concentration as in Table 3; all other parameter settings are standard (see Tables 1 and 2). *A*: $[Ca^{2+}]_i$; *B*: membrane potential. *C*: Ca^{2+} in ER ($[Ca^{2+}]_{ER}$). *D*: cytosolic ATP ($[ATP]_i$). *E*: cytosolic IP_3 ($[IP_3]_i$). *F*: intracellular Na^+ concentration ($[Na^+]_i$). For simulation of Tg action, the maximal rate of sarco(endo)plasmic reticulum (SERCA; P_{CaER}) was decreased from 0.105 to 0.013 μM/ms at *arrow 3* in *B*.

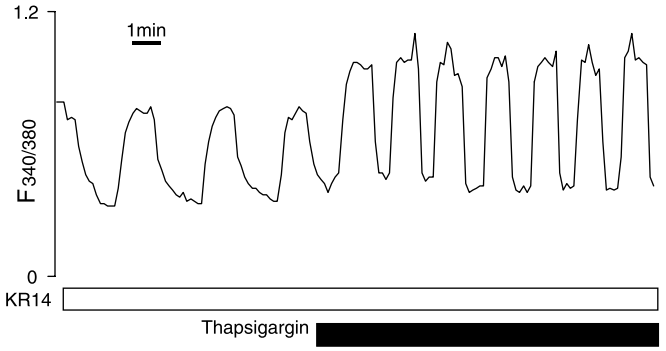

Fig. 2. Slow Ca^{2+} oscillations and effect of thapsigargin (Tg) in mouse islets. Mouse islets were loaded with fura 2-AM, and changes in $[Ca^{2+}]_i$ [expressed as the 340/380 nm ratio ($F_{340/380}$)] were recorded during 14 mM glucose and subsequent addition of 1 μM Tg (shown).

Dissection of the burst mechanism and the effects of Tg will be discussed in *Model Sensitivity to Slow Variables*.

Biphasic responses and fast Ca^{2+} oscillations. Fast oscillations usually show a more complex picture. In this case, the electrical response of pancreatic islets to step increases in glucose concentration is often biphasic, consisting of a prolonged depolarization with action potentials (Phase 1) followed by fast bursts of membrane potential and Ca^{2+} oscillations. The initial tonic electrical activity is accompanied by a sustained elevation of $[Ca^{2+}]_i$ (8, 72, 89).

It was suggested by model simulations and experimental results that the Phase 1 response may result from the combined influences of depolarizing K_{ATP} channel closure and I_{CRAN} deactivation. The Ca^{2+} fills the ER during Phase 1, deactivating I_{CRAN} and repolarizing the PM, allowing steady-state bursting to commence (8, 62). We are also able to simulate these results on the basis of our model when Ca^{2+} fills the ER to considerably elevated concentrations. This increase of $[Ca^{2+}]_{ER}$ can occur if Ca^{2+} output from the ER is restricted, for example, by closing IP_3R channels. This can be achieved in our model, for example, by decreasing the $[IP_3]_i$ as a consequence of decreased IP_3 production. The typical Phase 1 response followed by spike-burst behavior of the membrane potential and the fast oscillation patterns of ions and $[ATP]_i$ are illustrated in Fig. 4. It was simulated at a decreased IP_3 synthesis rate constant and an intermediate value of the rate constant of ATP_i production.

The same results can be simply obtained by a partial closing of the IP_3R channels in place of the decreased IP_3 production (not shown). Our model also shows that the duration of Phase 1 decreases with increased initial $[Ca^{2+}]_{ER}$ at $t = 0$ (not shown; see Ref. 62).

Simulating increased ATP_i production leads to increased oscillation frequency, progressing to continuous spiking with a further increase in the ATP_i production rate constant (Fig. 4). This is in reasonably good agreement with the experimental data (13, 37).

Note that fast $[Ca^{2+}]_i$ oscillations simulated by our model (Fig. 4) have an appearance very similar to those observed in pancreatic β-cells (8, 72). They also resemble the fast oscillations that were obtained in preceding models (8, 14, 62). This is not surprising, because our simulation of fast oscillations is close to those employed in these models.

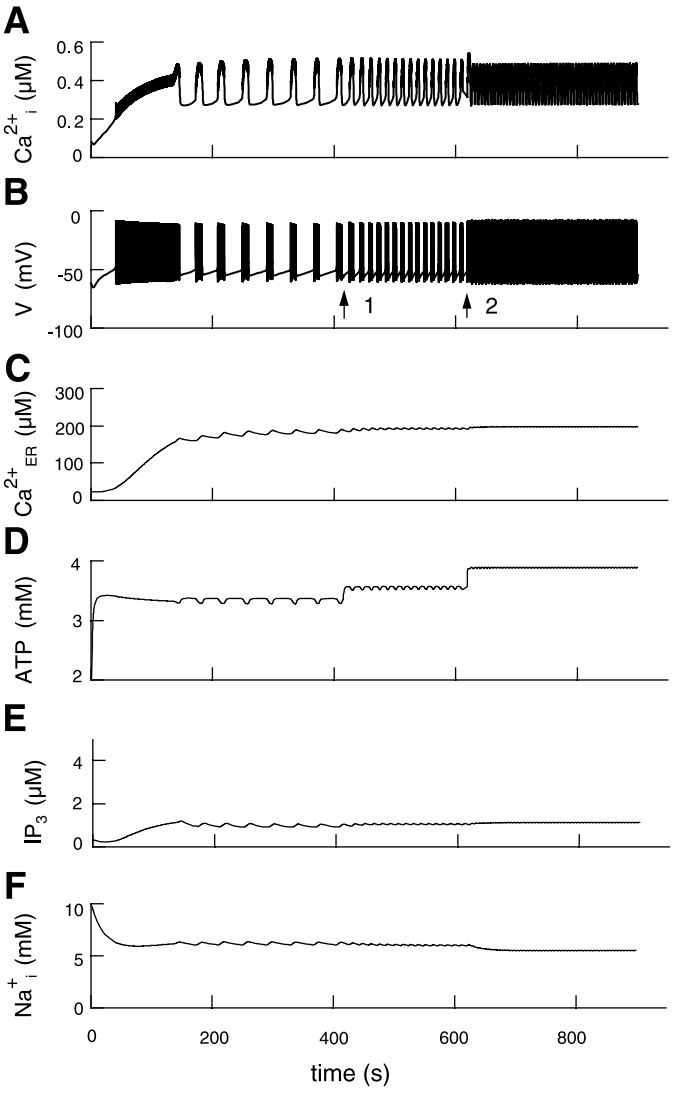

Fig. 4. Biphasic response to glucose in islets, simulated by increase of k_{ADP} from 0.03 to 0.45 s^{-1} at low rate of IP_3 synthesis (k_{IP} from *Eq. 21* is 0.1 instead 0.3 μM/s in Fig. 3) at $t = 0$. All other parameter settings are as in Fig. 3. For simulation of glucose addition at *arrow 1*, k_{ADP} was increased from 0.45 to 0.7 s^{-1} and at *arrow 2* from 0.7 to 2 s^{-1}.

Model Sensitivity to Slow Variables

Four parameters can change slowly in our model ($[ATP]_i$, $[Ca^{2+}]_{ER}$, $[IP_3]_i$, and $[Na^+]_i$), and their variations can lead to a slow membrane repolarization during a depolarized phase and to a depolarization in a silent phase. To determine the role of different processes and parameters, we performed an analysis of model sensitivity to slow variables to fix some parameters at their mean level for some kind of oscillations. It was found that the slow oscillations take place when only $[Na^+]_i$ ($[ATP]_i$, $[Ca^{2+}]_{ER}$, and $[IP_3]_i$ were constant) can change (Fig. 5*D*), and the characteristic fast oscillations occur when only $[Ca^{2+}]_{ER}$ ($[ATP]_i$, $[Na^+]_i$, and $[IP_3]_i$ were constant) can vary (Fig. 5*C*). Consideration of these two cases simplifies the general analysis.

The behavior of $[Ca^{2+}]_i$, V, $[Ca^{2+}]_{ER}$, $[IP_3]_i$, and $[Na^+]_i$ and the most essential current components is shown in Fig. 5, *A* and *B*, for single oscillations of slow and fast types. Because of the large fluctuations of I_{CRAN}, the voltage-independent part of this current (f_{CRAN}, *Eq. 12*) is also represented to facilitate the analysis (broken lines in Fig. 5.9). Corresponding concentrations and currents are also represented for cases when only $[Ca^{2+}]_{ER}$ (Fig. 5*C*) or $[Na^+]_i$ (Fig. 5*D*) can change. The contribution of other currents was either insignificant (I_{Na}) or does not change considerably between cases ($I_{Ca,pump}$, I_{KDr}, I_{KCa}, I_{KATP}).

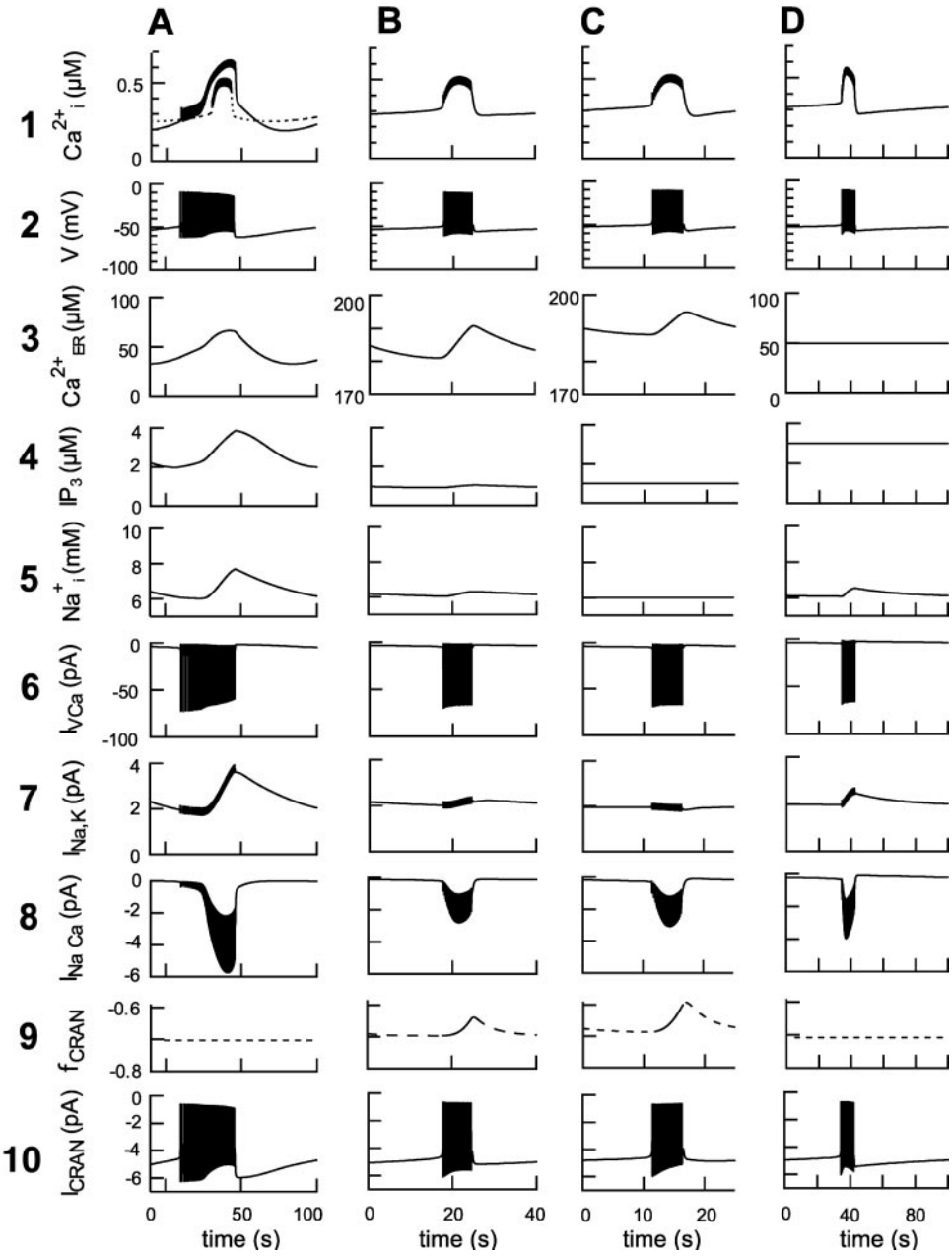

Fig. 5. Simulation of single oscillations. Model solutions were obtained from the oscillation pattern after simulation of glucose addition as in Figs. 3 and 4. Concentrations, PM potential, and some currents are represented for 1 characteristic oscillation. Broken lines in Fig. 5.9 correspond to a membrane potential-independent part of I_{CRAN} conductance (f_{CRAN}, *Eq. 12*). Units are shown in series, labeled in *A* with the exception of Fig. 5.3 for $[Ca^{2+}]_{ER}$, where units are shown for every case. *A*: single characteristic slow oscillation from Fig. 3 (*left*). Broken line in *A*.1 corresponds to a single $[Ca^{2+}]_i$ oscillation, when only $[IP_3]_i$ was fixed at its mean level (3 μM) with other parameters, as at the beginning of Fig. 3. *B*: single characteristic fast oscillation from beginning of Fig. 4. *C*: simulation of single characteristic oscillation determined only by $[Ca^{2+}]_{ER}$ changes at $k_{ADP} = 0.45\ s^{-1}$. Other slow variables were frozen at their mean level for fast oscillations in *B*: $[IP_3]_i = 1$ μM, $[Na^+]_i = 6$ mM, $[ATP]_i = 3.5$ mM. *D*: simulation of single characteristic oscillation determined only by $[Na^+]_i$ changes at $k_{ADP} = 0.37\ s^{-1}$. Other slow variables were frozen at their mean level for slow oscillation in *A*: $[IP_3]_i = 3$ μM, $[Ca^{2+}]_{ER} = 50$ μM, $[ATP]_i = 3.3$ mM.

ATP sensitivity. Activation of the Na^+/K^+ pump with increased $[Na^+]_i$ concentration during the depolarized phase accelerates ATP consumption in our model. Total Ca^{2+} pump rates and Ca^{2+}-dependent ATP_i consumption also increase during the depolarized phase with $[Ca^{2+}]_i$ rising (see *Eq. 27*). The acceleration of ATP_i consumption leads to a decreased $[ATP]_i/[ADP]_i$ ratio (Figs. 3 and 4). It is therefore possible that cyclic changes in the $[ATP]_i/[ADP]_i$ ratio control the cyclic closure and reopening of K_{ATP} channels. This has been proposed as a mechanism underlying the oscillatory behavior of β-cells (1, 65, 82).

We evaluated this possibility and found that fixing $[ATP]_i$ at a mean level yields no noticeable effect on the oscillatory pattern shown in Fig. 5, *A* and *B*. This can be explained by insignificant changes of the fraction of K_{ATP} channels open (APPENDIX C) during the ATP_i variations around its mean value (not shown). This suggests that $[ATP]_i$ is not the variable that drives slow oscillations in our model. On the other hand, considerable changes in mean $[ATP]_i$ and correspondingly in I_{KATP} can lead to a dramatic change in oscillations (see Figs. 3 and 4).

Single-oscillation analyses. It can be seen that spike activity is generated by the alternate activation of delayed rectifying K^+ channels and voltage-gated Ca^{2+} channels in every case. It is analogous to other models and has been previously analyzed (14, 78). The main difference between the models includes the nature of processes that lead to slow depolarization of PM poten-

tial during the depolarized phase and to its repolarizing during a silent phase.

When $[Ca^{2+}]_{ER}$ is the only slow parameter ($[ATP]_i$, $[Na^+]_i$, and $[IP_3]_i$ were constants; Fig. 5*C*), the following mechanism is responsible for oscillations: rising Ca_i^{2+} during the depolarized phase leads to increased Ca^{2+} pumping from the cytoplasm to the ER and to Ca_{ER}^{2+} accumulation, with corresponding closure of CRAN channels and decreased I_{CRAN}, that can be observed more clearly from the change of the voltage-independent part of I_{CRAN} (f_{CRAN}, broken line in Fig. 5*C*.9). This, in turn, leads to PM repolarization. These processes have opposite directions in the silent phase.

Figure 5*D* shows that, when $[Na^+]_i$ is the only slow variable ($[ATP]_i$, $[Ca^{2+}]_{ER}$, and $[IP_3]_i$ were constant), $I_{Na,K}$ is the main current that manages the slow PM potential changes leading to oscillations. The mechanism involves increased $[Ca^{2+}]_i$ during a depolarized period, activating the outward Ca^{2+} flux through Na^+/Ca^{2+} exchangers and a corresponding inward Na^+ flux. The resultant increase in $[Na^+]_i$ leads to the slow increase of outward current through electrogenic Na^+/K^+ pumps ($I_{Na,K}$; Fig. 5*D*.7) with corresponding PM repolarization. Falling $[Na^+]_i$ during a silent phase leads to decreased $I_{Na,K}$ and then in turn to PM depolarization.

In the simulation of slow oscillations shown in Fig. 5*A*, $[Na^+]_i$ and the current $I_{Na,K}$ change as in Fig. 5*D*, with no change of the voltage-independent part of the current I_{CRAN} (f_{CRAN}). Correspondingly, the mechanism of slow oscillations is the mechanism described above, with $[Na^+]_i$ as the only slow variable.

In the simulation of fast oscillations shown in Fig. 5*B*, $[Ca^{2+}]_{ER}$ and f_{CRAN} change as in Fig. 5*C*, with little change of $[Na^+]_i$ and the corresponding current $I_{Na,K}$. In this case, the currents $I_{Na,K}$ and I_{CRAN} act together. However, I_{CRAN} plays the major part, as the concentrations and currents are similar in Fig. 5, *B* and *C*. This is in agreement with the conclusion that $[Ca^{2+}]_{ER}$ drives the fast oscillations but does not need to oscillate to have slow oscillations, whereas $[Na^+]_i$ gives slow oscillations but does not need to oscillate to have fast oscillations.

However, in the case of fast oscillations, CRAN channels are working under conditions when the ER is filled with Ca^{2+}, and the $[Ca^{2+}]_{ER}$ change occurs close to the half-activation level of $[Ca^{2+}]_{ER}$ for CRAN channels (200 μM; see *Eq. 12* and Table 1). This leads to an increased rate of both PM potential depolarization and repolarization, when $[Ca^{2+}]_{ER}$ correspondingly increases and decreases following $[Ca^{2+}]_i$ changes.

Shape of slow $[Ca^{2+}]_i$ oscillations and role of IP_3. It can be seen in our simulations that, at the beginning of the silent period of slow oscillations, Ca_{ER}^{2+} is gradually released into the cytosol (Figs. 3 and 5*A*.3) and the shape of the $[Ca^{2+}]_i$ curve is close to what was found by us (Fig. 2) and others (27, 83) in experiments. Such a slow phase is absent at the simulation of fast oscillations (Figs. 3 and 5*B*.1).

When $[IP_3]_i$ was fixed at its mean level at the conditions that were used to simulate slow oscillations, there was still the ability to produce some oscillations. However, the slow $[Ca^{2+}]_i$ decrease disappears at the beginning of the silent period. This resulting single $[Ca^{2+}]_i$ oscillation is shown as a broken line in Fig. 5*A*.1.

The relationship between $[Ca^{2+}]_i$ and $[Ca^{2+}]_{ER}$ needs additional clarification. In our model, a dynamic equilibrium is established between $[Ca^{2+}]_i$ and $[Ca^{2+}]_{ER}$ for several seconds when there is no spiking activity; that is, $[Ca^{2+}]_i$ and $[Ca^{2+}]_{ER}$ are closely connected. The decrease in $[IP_3]_i$ leads to a corresponding, slow IP_3R channel closure that decreases the rate of Ca^{2+} flux from the ER. A slow $[Ca^{2+}]_{ER}$ drop leads to a slow decrease in $[Ca^{2+}]_i$ at their dynamic equilibrium. When the $[IP_3]_i$ is fixed, this mechanism does not operate, and the slow $[Ca^{2+}]_i$ drop disappears.

No remarkable changes in the fast oscillations pattern (shown in Fig. 5*B*) were observed if $[IP_3]_i$ was fixed at its mean level with otherwise identical conditions (not shown). The lack of an effect can be understood in light of the small changes in $[IP_3]_i$ that occur during fast oscillations (see Figs. 4 and 5*B*.4).

This suggests that changes in $[IP_3]_i$ are not the main driving force for the fast and slow oscillations in our model. However, the change of mean $[IP_3]_i$ can have a considerable effect, including a transformation of slow oscillations to fast at decreasing $[IP_3]_i$ (compare Figs. 3 and 4). Furthermore, $[IP_3]_i$ changes can have a considerable effect on the pattern of slow oscillations.

Role of the ER. In islets pretreated with Tg to block the SERCA pump, the frequency was increased, the amplitude of slow $[Ca^{2+}]_i$ oscillations was larger than in control islets, and the descending phase of each $[Ca^{2+}]_i$ oscillation was fast with no slow descending second phase (Fig. 2; see also Refs. 27, 64).

Our model permits a simulation of these experiments (Fig. 3). In this case, the corresponding amplitude of slow $[Ca^{2+}]_i$ oscillations was larger, the period of oscillation was shorter, and the descending phase of each $[Ca^{2+}]_i$ oscillation was fast with no slow second phase (Fig. 3), all of which are in reasonably good agreement with the experimental data.

In this case, Ca^{2+} in the ER does not drive the oscillations. However, the remaining $[Na^+]_i$-dependent mechanisms are able to create the relevant oscillations, and corresponding fluxes resemble the ones that were observed if the oscillations were driven only by Na_i variations, as in Fig. 5*D*.

A different pattern was found when SERCA pumps were blocked in fast oscillation experiments. Worley et al. (89) observed that, when Tg was added to the medium, the bursting was transformed to continuous spiking, and fast $[Ca^{2+}]_i$ oscillations were converted to a tonically elevated Ca^{2+} level. Bertram et al. (8) found that an addition of Tg was accompanied by a gradual increase in the plateau fraction and in electrical burst frequency.

However, in our general model, blocking of SERCA leads to the pattern of slow oscillations, as shown in Fig. 3, *right*. For this reason, other possibilities were investigated. When oscillations were simulated only by

changes in $[Ca^{2+}]_{ER}$ (by fixing $[Na^+]_i$, $[IP_3]_i$, and $[ATP]_i$ to constant values, as in Fig. 5*C*), the block of the SERCA pumps increased the frequency of fast $[Ca^{2+}]_i$ oscillations, because I_{CRAN} is activated in consequence of $[Ca^{2+}]_{ER}$ decrease. A further increase of SERCA inhibition can then lead to a permanent PM depolarization and to a continuous rise in $[Ca^{2+}]_i$ (Fig. 6). This transformation is consistent with the aforementioned experiments for fast oscillations. It is also in agreement with the results of the modeling of Chay (14) and Bertram et al. (8), who had not included $[Na^+]_i$ changes in their models and had taken into account only Ca^{2+} and K^+ currents and $[Ca^{2+}]_{ER}$ influence on I_{CRAN}.

In other words, the model suggests that, under conditions when fast oscillations occur, something is blocking the $[Na^+]_i$-dependent oscillation mechanisms, even though Tg action resulted in a depletion of the Ca_{ER} store. One possible mechanism is a partial inhibition of the Na^+/K^+ pump. For example, we found that only $[Ca^{2+}]_{ER}$-dependent fast oscillations were possible in our model when the maximum activity of the Na^+-K^+-ATPase was diminished to 25% of basal activity, even though all other coefficients and initial concentrations were as in Fig. 4. In this case, a simulation of Tg action at fast oscillations resembles Fig. 6. However, the physiological differences between fast and slow oscillations need further examination.

Role of $[Na^+]_i$. Slow glucose-induced $[Na^+]_i$ oscillations were found in individual β-cells under conditions known to induce oscillations of $[Ca^{2+}]_i$ (34, 35). Partial suppression of the Na^+/K^+ pump by ouabain resulted in an increased amplitude of slow Na^+ and Ca^{2+} oscillations and decreased their frequency. Slow $[Na^+]_i$ and $[Ca^{2+}]_i$ oscillations were converted to tonically elevated $[Na^+]_i$ and $[Ca^{2+}]_i$ levels following increased ouabain concentration (34, 35).

Our simulation leads to analogous results (Fig. 7). This result can be explained on the basis of our model: the partial suppression of the Na^+/K^+ pump leads to decreased $I_{Na,K}$, which is responsible for slow PM potential variations. For this reason, to obtain the same value of $I_{Na,K}$ variation that leads to a corresponding PM potential change, it was necessary to have larger $[Na^+]_i$ changes. This extends the time necessary for corresponding $[Na^+]_i$ accumulation or dissipation. The increase in Na^+/K^+ pump inhibition leads to collapse of this $[Na^+]_i$-connected mechanism and to the disappearance of slow oscillations.

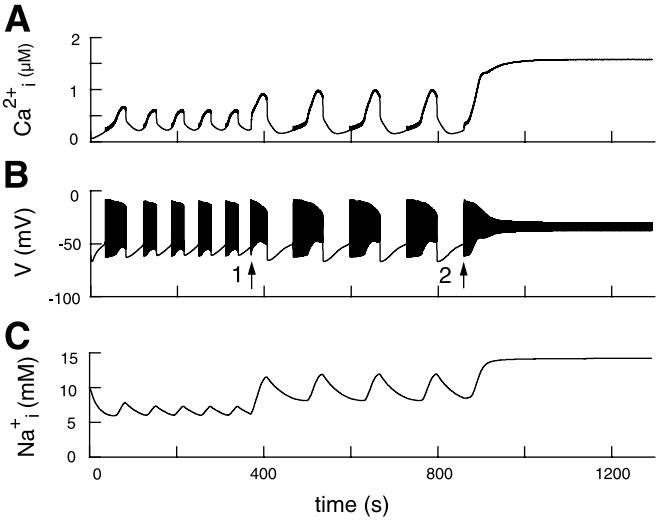

Fig. 7. Simulated applications of ouabain to a cell that exhibits slow oscillations with the initial simulation as in Fig. 3. Addition of ouabain is modeled by decreasing P_{NaK} from 600 to 200 fA (*arrow 1*) in *B* and from 200 to 150 fA (*arrow 2*).

To check the role of $[Na^+]_i$ in driving slow oscillations, we also froze $[Na^+]_i$ at its mean level characterized for slow oscillations (7 mM) and made a simulation at the initial conditions by using the coefficients characterized for slow oscillations (as in Fig. 3). No oscillations were found (not shown).

Our model simulations demonstrate the necessity for $[Na^+]_i$ oscillations to drive the slow Ca^{2+} oscillations and suggest that $[Na^+]_i$ is a candidate pacemaker for slow oscillations.

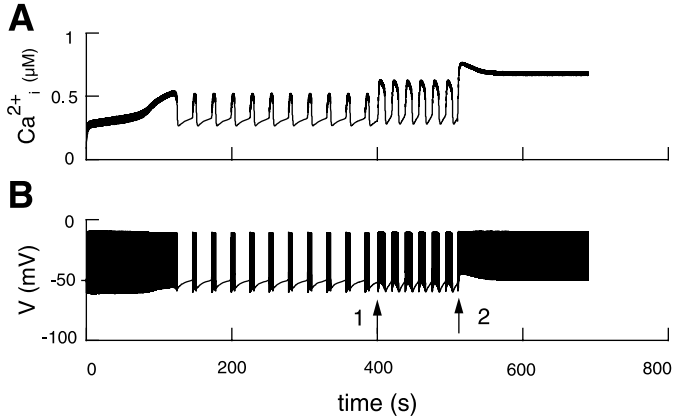

Fig. 6. Model simulation of Tg action on fast oscillations at k_{ADP} = 0.45 s^{-1} with the initial simulation as in Fig. 4 and frozen concentrations of $[ATP]_i$, $[Na^+]_i$, and $[IP_3]_i$ as in Fig. 5*C*. Maximal rate of SERCA (P_{CaER}) was decreased from 0.105 to 0.0785 μM/ms at *arrow 1* in *B* and from 0.0785 to 0.0524 μM/ms at *arrow 2*.

β-Cell Lines

We have previously studied the properties of a clonal β-cell line termed βTC3-neo (74). In contrast to normal mouse islets, this cell line does not usually respond to a step increase in glucose concentration with regular oscillatory increases in $[Ca^{2+}]_i$. Instead, a slow rise in $[Ca^{2+}]_i$ occurs with occasional intermittent spikes. However, the exposure of βTC3-neo cells to 20 mM TEA, a blocker of K^+ channels (24), permitted the generation by glucose of large, regular, slow oscillations in $[Ca^{2+}]_i$. In the absence of glucose, TEA was without effect (74). However, the molecular differences between βTC3-neo cells and primary β-cells have not been completely studied.

The magnitude of the Ca^{2+} inward current in β-cells within intact pancreatic islets is considerably more than in individual β-cells maintained in tissue culture [up to twice (33)]. This difference can be expected to have dramatic effects on the generation of β-cell elec-

trical activity and leads to failure of dispersed cells to generate the characteristic oscillatory electrical activity (33, 81). It is reasonable to assume that βTC3-neo cells also have a decreased Ca^{2+} inward current that can be simulated by a reduced conductance of Ca^{2+} channels in our model.

Under these conditions, i.e., reduced conductance of Ca^{2+} channels, simulation of glucose addition does not lead to oscillations. However, a partial block of delayed-rectifier K^+ channels, small-conductance Ca^{2+}-activated K^+ channels, and K_{ATP} channels, which simulate TEA action, leads to large, regular oscillations in our model (Fig. 8). This occurs because the decreased inward Ca^{2+} current leads to PM repolarization. To restore the possibility of oscillations, a corresponding decrease of K^+ outward currents, as by TEA action, is required to allow PM depolarization.

The exposure of βTC3-neo cells to 1 μM nitrendipine, which blocks L-type Ca^{2+} channels, can reversibly suppress oscillatory activity (Fig. 1*C* in Ref. 74). In our model, a similar decrease in Ca^{2+} channel activity also leads to a suppression of oscillatory activity (not shown).

In the absence of glucose, exposure of βTC3-neo cells to 100 μM tolbutamide to block I_{KATP} induced $[Ca^{2+}]_i$ oscillations only in the presence of TEA (Fig. 2*A* in Ref. 74). The same results were obtained with our model (Fig. 9) when an additional block of K_{ATP} channels was used to simulate tolbutamide effects. In this case, the simulation of tolbutamide addition on I_{KATP} was equivalent to the simulation of glucose additions in Fig. 8.

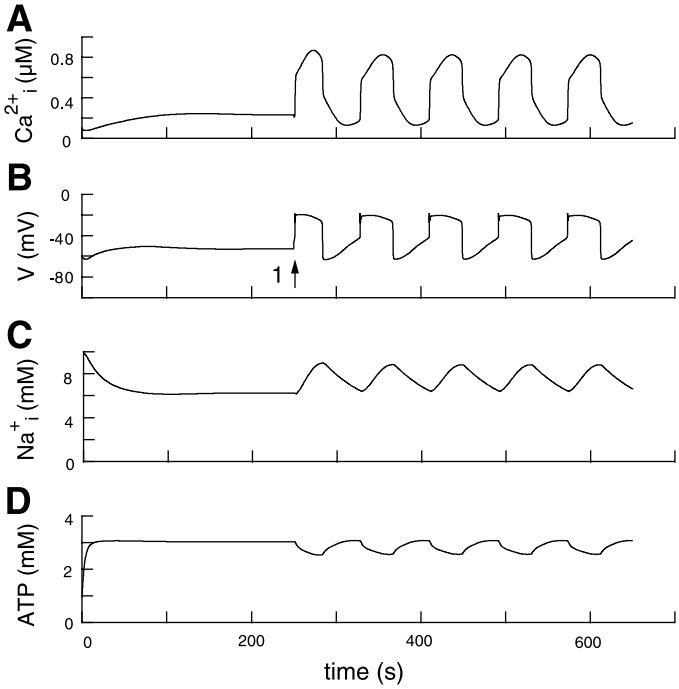

Fig. 8. Model simulation of a β-cell line experiment at intermediate glucose level was made at a step increase of rate constant of ATP production from low to intermediate value (from k_{ADP} = 0.03 to 0.25 s^{-1}) at t = 0; all other parameter setting are standard (see Tables 1–3), with the exception of g_{mVCa} for voltage-activated Ca^{2+} current that was decreased from 770 to 300 pS. For simulation of tetraethylammonium (TEA) action at *arrow 1*, maximal conductance for K^+ channels was decreased: for K_{ATP} from 24,000 to 12,000 pS, for a delayed rectifier K^+ current from 3,000 to 800 pS, and for the voltage-independent small conductance Ca^{2+}-activated K^+ current from 130 to 60 pS.

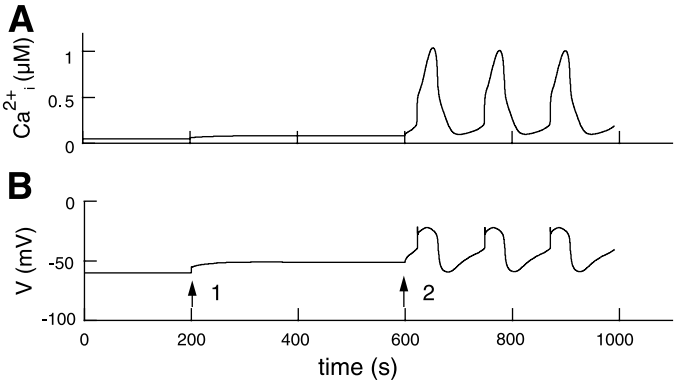

Fig. 9. Model simulation of a β-cell line experiment at a low glucose level (k_{ADP} = 0.03 s^{-1} for all time) and the additional action of TEA and tolbutamide. To simulate TEA action, coefficients were taken as in Fig. 8*B* at *arrow 1*. To simulate tolbutamide action, maximal conductance for K_{ATP} was decreased from from 12,000 to 4,000 pS at *arrow 2*.

Similar experimental results were obtained by Eberhardson and Grapengiesser (21) for single β-cells isolated from mouse islets, in which the $[Ca^{2+}]_i$ oscillations could be obtained at low glucose concentration only when both TEA and tolbutamide were added.

DISCUSSION

We have attempted to integrate plasma membrane and intracellular events in modeling the behavior of pancreatic β-cells by building on several previous models. The model includes consideration of ionic flux, metabolism, and regulation by intracellular messengers. The complexity of the system necessarily left us with some flexibility in assigning values of the parameters. Therefore, it would be unreasonable to expect the model to accurately reproduce all previously observed experimental results. However, it is necessary to verify that the model is able to reproduce the general features of β-cell or islet oscillation patterns.

Islet Oscillatory Behavior

The majority of previous models emphasized the features of fast-type oscillations, and detailed theoretical considerations of this kind of oscillations have been made (14, 26, 62, 65, 78). We were also able to simulate these fast oscillations (Figs. 4 and 5*B*). Slow oscillations most likely constitute a physiological oscillatory pattern in β-cells, and they may constitute the framework for pulsatile insulin release observed in vivo (28, 37). For this reason, an explanation for this type of oscillation in islets and β-cell lines is the main aim of this article.

It is critical to determine the degree of correlation between observed and simulated β-cell behavior. Several recent studies in the literature have shown addi-

tional experimental results consistent with the model that we present here, even though the authors' own interpretation is not identical to our model results. For example, K_{ATP} channel data (51) and data on glucose concentrations and oxygen consumption (2, 17) suggest that the ATP/ADP ratio may indeed oscillate on a time scale appropriate for the generation of slow oscillations. It was found that the ATP/ADP ratio drops rapidly when $[Ca^{2+}]_i$ is raised and increases when $[Ca^{2+}]_i$ falls (2, 19). These results are consistent with our calculations of $[ATP]_i$ behavior (Fig. 3). However, it should be pointed out that the $[Ca^{2+}]_i$-dependent changes in the ATP/ADP ratio are not driving oscillations in our model.

The assumption that $[IP_3]_i$ can oscillate concomitantly with $[Ca^{2+}]_i$ has received recent experimental support by the indirect demonstration of IP_3 oscillations in ATP-stimulated Madin-Darby canine kidney epithelial cells (42). For murine β-cells in suspension, the intracellular IP_3 level oscillated approximately in synchrony with changes in $[Ca^{2+}]_i$ when driven by the sequential addition of glucose, an α_2-adrenergic stimulus, and extracellular Ca^{2+} (5). It was also shown in RESULTS that our simulations are also consistent with data for $[Na^+]_i$ oscillations.

All of these data are in reasonably good agreement with our model. However, it is important to emphasize that, although the modeled voltage and ion dependences are consistent with available data, the simultaneous measurements of the voltage dependence, relative conductance of different channels, and $[Ca^{2+}]_i$, $[ATP]_i$, $[Na^+]_i$, $[Ca^{2+}]_{ER}$, and $[IP_3]_i$ oscillations have not been directly demonstrated and need to be tested.

In addition, it should be pointed out that large oscillations in $[ATP]_i$, $[Ca^{2+}]_{ER}$, $[Na^+]_i$, and $[IP_3]_i$ should only be forthcoming in the slow $[Ca^{2+}]_i$ oscillations, as was calculated above (Figs. 3, 5*A*, and 7). Fast $[Ca^{2+}]_i$ oscillations can follow very small changes in other components (Figs. 4 and 5*B*), and it can be very difficult to measure these changes.

β-Cell Modeling: Identity of Slow Variables

Several types of models can explain electrical bursting and $[Ca^{2+}]_i$ oscillations in β-cells. All known models have negative feedback from a slow variable driving the oscillations but differ in the identity of what the slow variable might be.

The first β-cell models were based on the hypothesis that the $[Ca^{2+}]_i$ is the slow variable, influencing the membrane through a Ca^{2+}-activated K^+ current. However, the spectrophotometric measurements show that the time scale of the $[Ca^{2+}]_i$ change is short relative to the oscillation period (see Refs. 26 and 78 for details). For this reason, we have not created a model in which $[Ca^{2+}]_i$ is a possible driving slow variable.

The possibility that the ATP/ADP ratio is the slow variable driving electrical bursting by acting on the K_{ATP} channel was modeled by several investigators (46, 65, 82). However, the bursts and $[Ca^{2+}]_i$ oscillations were principally obtained with a time constant appropriate for fast bursting in these models. Furthermore, it was shown in Refs. 74 and 75 that bursting and $[Ca^{2+}]_i$ oscillations persist in the presence of a K_{ATP} channel blocker under conditions where I_{KATP} is substantially decreased. This fact argues against a critical role for oscillations in K_{ATP} channels in these processes. We have also shown that, despite the fact that the change of mean ATP concentration can induce the oscillations or change their pattern, the ATP/ADP oscillation is not the driving force of $[Ca^{2+}]_i$ oscillations in our model.

Several models have been proposed in which the dynamics of Ca^{2+} in the ER serves as the slow variable driving bursting (8, 13, 14, 26, 62). The I_{CRAN} modifies the oscillation period and membrane potential in these models. We also followed these proposals for modeling fast oscillations. Our previous considerations (in RESULTS) showed that the dynamics of Ca^{2+} in the ER could be responsible for creating corresponding fast oscillations at a relatively high Ca^{2+}_{ER} level, where there is a significant influence of $[Ca^{2+}]_{ER}$ changes on I_{CRAN}.

Although these models (8, 13, 14, 26, 62) have been applied mainly to an analysis of fast oscillations, this mechanism was also used for the generation of slow oscillations. Slow $[Ca^{2+}]_i$ oscillations were obtained by Chay (14) at a decreased coefficient of $Ca^{2+}{}_{ER}$ release from the ER. This retards the processes connected with Ca^{2+}_{ER} dynamics and, in turn, transforms fast oscillations to slow. Increased $[Ca^{2+}]_{ER}$ accompanies a decreased Ca^{2+} release from the ER. This means that the slow oscillations were generated at relatively high $[Ca^{2+}]_{ER}$ in the model (14), contrary to our results. Emptying of the ER leads to termination of both fast and slow oscillations in the Chay model.

Arguments have been made against the Ca^{2+}_{ER}-dependent model for slow oscillations, since it seems to be at odds with data demonstrating that slow oscillations persist in the presence of Tg (6, 54, 64), an agent that blocks SERCA and empties the ER stores. These data were also analyzed above (in RESULTS), where we demonstrated that SERCA block can eliminate fast oscillations, while leaving intact the mechanism creating slow oscillations via the change in $[Na^+]_i$ oscillations. For this reason, an expansion of the Ca^{2+}_{ER}-dependent model for fast oscillations to slow oscillations made by Chay (14) appears unjustified.

Recently, a Ca^{2+}-sensitive K^+ conductance was isolated that activates with a time constant of 2.3 s and inactivates with a time constant of 6.5 s in response to stimuli during voltage clamp (32). The authors concluded that that current, similar to a Ca^{2+}-activated K^+ current, played an important role in the generation of β-cell oscillatory activity. However, these time constants can only correspond to the fast oscillations.

Goforth at al. (31) have developed a new model to explain this slow K^+ current, where $[Ca^{2+}]_{ER}$ is also taken as the initial slow variable driving bursting. They introduced a new cytoplasmic Ca^{2+} pool localized between the ER and PM. Ca^{2+} released from the ER goes first to this intermediate Ca^{2+} pool. The changes of $[Ca^{2+}]_i$ in this intermediate Ca^{2+} pool serve in this

model to modulate the current through the Ca^{2+}-activated K^+ channels. We note also that the the value for the half-activation Ca^{2+} concentration assumed by Goforth at al. is much higher (0.7 μM) than that for the SK3 channels included here (0.1 μM).

However, Goforth at al. (31) chose this half-activation Ca^{2+} concentration arbitrarily to fit their model, specifically to address a potential high $[Ca^{2+}]_i$ pool in the sub-PM region. Although such a Ca^{2+} pool has been proposed for excitatory cells, it has not been directly shown in β-cells, nor has the "real" value of the half-activation Ca^{2+} concentration for KCa channel in β-cells been determined. Kanno et al. (44) also suggest that this slow K^+ current is determined not only by KCa channels. They found that activation and a reactivation of K_{ATP} channels can play a fundamental role in this slow K^+ current in intact mouse pancreatic islets.

In addition, as was discussed above, every model of slow oscillations based on the proposal that $[Ca^{2+}]_{ER}$ is the slow variable driving oscillations seems to be at odds with data demonstrating that slow oscillations persist in the presence of agents that block SERCA and empty the ER stores. This would restrict application of the Goforth et al. model to fast oscillations.

A very detailed model was developed by Magnus and Keizer (58, 59). They proposed (and simulated) that Ca^{2+} in mitochondria is the main regulator of the mitochondrial membrane potential, thus affecting ATP synthesis and corresponding $[Ca^{2+}]_i$ oscillations. However, the view that mitochondrial change of calcium regulates ATP production under physiological conditions has been questioned (2, 27), and experimental support is still incomplete for the idea that changes in the ATP/ADP ratio are the main driving mechanism for all Ca^{2+} oscillations (see above).

Despite the clear evidence that IP_3 is one of the critical cellular messengers inducing Ca^{2+} mobilization from intracellular stores (38), IP_3 kinetics have not previously been included in the models of the pancreatic β-cell. Our model produced a simulation with a good match to data reported from several laboratories. The simulations also underlined how the IP_3 concentration was critical to understanding the pattern of slow $[Ca^{2+}]_i$ oscillations even though IP_3 does not account for the mechanism of oscillations.

Our simulations suggest that the change in $[Na^+]_i$ is one of the most important slow variables that govern slow $[Ca^{2+}]_i$ oscillations. Kitasato et al. (47) proposed such a role for Na^+. According to these authors, an increase in $[Ca^{2+}]_i$ results in an increase in $[Na^+]_i$ because of Na^+/Ca^{2+} exchanger activity. The increase in cytosolic Na^+ results in enhanced ATP consumption at Na^+/K^+ pump sites and in a decreased ATP/ADP ratio, which in turn could lead to activation of K_{ATP} channels followed by membrane repolarization. A decrease in $[Ca^{2+}]_i$ results in the opposite order of events during a silent phase. This scenario was modeled by Miwa and Imai (65) as the underlying mechanism of $[Ca^{2+}]_i$ oscillations. However, this mechanism does not explain the experimental data suggesting that ATP/ADP ratio changes are not the main driving force for $[Ca^{2+}]_i$ oscillations (see above).

Our model simulates an increase in $[Na^+]_i$ and a corresponding decrease in $[ATP]_i$ during the depolarized phase by use of a similar mechanism. However, our model shows that an increase of $[Na^+]_i$ during the depolarized phase and a corresponding increase of outward current through Na^+/K^+ pumps could be sufficient for PM repolarization that leads to transition to silent phase, even though a change of ATP concentration is not directly driving oscillations.

Slow oscillations of PM potential and $[Ca^{2+}]_i$ were obtained in previous models (e.g., Refs. 7 and 78) by introducing a special slow variable that does not have a clear metabolic basis. Our work is an attempt to find some real metabolic basis for this suggestion. According to our analysis, the Na^+ concentration in the cytoplasm may be the desired slow variable.

We also found that some coefficients used in previous models do not always correspond to physiological mechanisms. It has been suggested in previous models that Ca^{2+} is removed from the cytoplasm only by sequestration mechanisms that do not create any PM currents. For example, in one model (13), the mitochondrion sequesters intracellular Ca^{2+} with a rate constant of 3,000 s^{-1}, and this calcium is not recycled to the cytoplasm. In other examples, the Ca^{2+} removal rate through the PM (e.g., by sequestration in secretory granules) was assigned the following coefficients: 120 s^{-1} (82), 190 s^{-1} (58), and 640 s^{-1} by Gall and Susa (26) in their models II and III. This means that, in all of these models, total cytoplasmic Ca^{2+} disappears from the β-cells in only seconds as the result of mechanisms that do not create any current through the PM. We could not find any data to support such a significant flux created by sequestration mechanisms. Ca^{2+} is removed mainly by well-known PM Ca^{2+} pumps in our model that create a corresponding PM current (*Eq. 8*). The coefficient for the sequestration rate of Ca^{2+} through the PM (k_{sg} in *Eq. 24*) was estimated in our models as 0.1 s^{-1}, and we consider this to be a more reasonable value.

In the model by Miwa and Imai (65), only Na^+/K^+ active transporters and the Ca^{2+} pumps on the PM were employed to simulate ATP consumption in β-cells. Furthermore, the rate constant of ATP production from ADP was ~0.03 s^{-1} at high glucose levels. Other ATP consumption mechanisms exist in cells, which we simulate in our model (*Eq. 27*). The rate constant of ATP production from ADP was also considerably increased in our model (up to 10 times in Fig. 3) to be in agreement with experimental observations of ATP production rate (see MATERIALS AND METHODS). Furthermore, no flux analysis or analysis of oscillations at fixed values of ATP concentrations was made in (65). On the basis of simulations in our model, it seems possible that, in the model of Miwa and Imai, a change of Na^+ concentration also can directly effect PM potential by a change of $I_{Na/K}$.

Several additional slow variables can also take part in the regulation of oscillations in β-cells. For example,

the concentrations of such ions as K^+ and Cl^- were used as independent variables in the model (65). Unquestionably, K^+ concentration in the cytoplasm is very important. However, all cells, including β-cells, have 100–130 mM K^+ concentration in the cytoplasm, and its relative change must be small, particularly during fast oscillations (65). For this reason, we did not include K^+ cytoplasmic concentration as an independent variable in this model. It has also been found that glucose stimulation of the β-cells is coupled to an increase in their Cl^- permeability and that the oscillatory Ca^{2+} signaling may be critically dependent on transmembrane Cl^- fluxes (22). It seems plausible that additional kinetic equations for K^+, Cl^-, and other ions and their channels may become necessary for this model in the future to include emerging aspects of β-cell physiology.

In conclusion, our results support the hypothesis that it is necessary to include all essential ionic channels and pumps that have been identified in β-cells to employ mathematical models to correctly simulate the set of experimental results. Results from the simulations support the hypothesis that $[Ca^{2+}]_{ER}$ and $[Na^+]_i$ can be the main variables driving both fast and slow $[Ca^{2+}]_i$ oscillations and that the regulation of Ca^{2+} leak from the ER by IP_3 is also important to explain the pattern of slow calcium oscillations. The results of the modeling favor a scenario where two or more slow variables interact to produce oscillations, in agreement with other recent models (6, 7). On the basis of our analysis, it seems likely that differences in relative activity of channels and pumps could explain the variations in the electrical bursts and $[Ca^{2+}]_i$ oscillations between the islets, cell lines, and single β-cells.

APPENDIX A: NA^+/K^+ ACTIVE TRANSPORT

The general model (12) was employed in a modified form according to Miwa and Imai (65).

$$I_{Na,K} = P_{NaK}(F_1f_2f_3F_4F_5f_6 - b_1B_2B_3B_4b_5B_6)/D \qquad (A1)$$

where

$$D = f_2f_3F_4F_5f_6 + b_1f_3F_4F_5f_6 + b_1B_2F_4F_5f_6 + b_1B_2B_3F_5f_6 + b_1B_2B_3B_4f_6 + b_1B_2B_3B_4b_5$$

$F_1 = f_1[Na^+]_i^3$, $F_4 = f_4[K^+]_o^2$, $F_5 = f_5[ATP]_i$, $B_2 = b_2[ADP]_i$, $B_3 = b_3[Na^+]_o^3$, $B_4 = b_4[P]$, $B_6 = b_6[Ksup+]_i^2$, $f_5 = f_5^* \exp \times (VF/2RT)$, $b_5 = b_5^* \exp(-VF/2RT)$

where P_{NaK} is a coefficient for resulting current in the presence of saturating level of ATP; [P] is an inorganic phosphate concentration; b_1, b_2, b_3, b_4, b_5^*, b_6, f_1, f_2, f_3, f_5^*, and f_6 are the rate coefficients: [P] = 4,950 μM, $f_1 = 2.5\ 10^{-10}\ \mu M^{-3}\ ms^{-1}$, $f_2 = 10\ ms^{-1}$, $f_3 = 0.172\ ms^{-1}$, $f_4 = 1.5\ 10^{-8}\ \mu M^{-2}\ ms^{-1}$, $f_5^* = 0.002\ \mu M^{-1}\ ms^{-1}$, $f_6 = 11.5\ ms^{-1}$, $b_1 = 100\ ms^{-1}$, $b_2 = 0.0001\ \mu M^{-1}\ ms^{-1}$, $b_3 = 1.72\ 10^{-17}\ \mu M^{-3}\ ms^{-1}$, $b_4 = 0.0002\ \mu M^{-1}\ ms^{-1}$, $b_5^* = 0.03\ ms^{-1}$, $b_6 = 6\ 10^{-7}\ \mu M^{-1}\ ms^{-1}$).

Rate constants were taken as proposed in Refs. 12 and 65 (for f_5^* and b_5^* see *curve B* in Fig. 3 from Ref. 12). P_{NaK} was estimated to fit the experimental data (Table 1).

APPENDIX B: GENERAL GATING VARIABLE FOR I_{KDR}

According to Gall and Susa (26) and Sherman (78), the general gating variable for I_{KDr} can be determined as

$$\frac{dn}{dt} = \frac{n_\infty(V) - n}{\tau_n(V)} \qquad (B1)$$

where

$$n_\infty(V) = \frac{1}{1 + \exp[(V_n - V)/S_n)]} \qquad (B2)$$

$$\tau_n(V) = \frac{c}{\exp[(V - V_\tau)/a] + \exp[(V_\tau - V)/b]} \qquad (B3)$$

where n_∞ is the steady-state value of the general gating variable, V_n is the half-activation potential, S_n is the slopes at half-maximal potential, $\tau_n(V)$ is the relaxation time constant, a, b, c, and V_τ are the adjustable coefficients. The coefficients were fitted on the basis of previous models (26, 82): $V_n = -14$ mV, $S_n = 7$ mV, a = 65 mV, b = 20 mV, c = 20 ms, and $V_\tau = -75$ mV.

APPENDIX C: FRACTION OF K_{ATP} CHANNELS OPEN

For the fraction of K_{ATP} channels open, we adopt a detailed kinetic model that was created by Magnus and Keizer (58) and that was based on the results of Ref. 43. The equation for the fraction of open channels can be included on the basis of that model if we take into account the parameters determining adenine nucleotide concentrations (see Table 2 from Ref. 58). Then the resulting fraction of K_{ATP} channels open has the form

$$O_{KATP} = \frac{0.08(1 + 0.33[ADP]_i/K_{dd}) + 0.89(0.165[ADP]_i/K_{dd})^2}{(1 + 0.165[ADP]_i/K_{dd})^2\,(1 + 0.135[ADP]_i/K_{td} + 0.05[ATP]_i/K_{tt})} \qquad (C1)$$

O_{KATP} is the fraction of channels open. K_{dd}, K_{td}, and K_{tt} are the dissociation constants ($K_{dd} = 17$ μM, $K_{td} = 26$ μM, and $K_{tt} = 1$ μM). According to Hopkins et al. (43), *Eqs. 19* and *C1* reproduce well the experimental data.

We thank A. Kuznetsov and M. Roe for helpful discussions.

This work was partially supported by National Institute of Diabetes and Digestive and Kidney Diseases Grants DK-44840, DK-20595, and DK-48494, and the Blum-Kovler Foundation.

REFERENCES

1. **Ainscow EK and Rutter GA.** Mitochondrial priming modifies Ca^{2+} oscillations and insulin secretion in pancreatic islets. *Biochem J* 353: 175–180, 2001.
2. **Ainscow EK and Rutter GA.** Glucose-stimulated oscillations in free cytosolic ATP concentration imaged in single islet β-sells: evidence for a Ca^{2+}-dependent mechanism. *Diabetes* 51: S162–S170, 2002.
3. **Allen V, Swigart P, Cheung R, Cockcroft S, and Katan M.** Regulation of inositol lipid-specific phospholipase cδ by changes in Ca^{2+} ion concentrations. *Biochem J* 327: 545–552, 1997.
4. **Ashcroft FM and Rorsman P.** Electrophysiology of the pancreatic β-cell. *Prog Biophys Mol Biol* 54: 87–143, 1989.
5. **Barker CJ, Nilsson T, Kirk CJ, Michell RH, and Berggren PO.** Simultaneous oscillations of cytoplasmic free Ca^{2+} concentration and $Ins(1,4,5)P_3$ concentration in mouse pancreatic β-cells. *Biochem J* 297: 265–268, 1994.
6. **Bertram R and Sherman A.** Dynamical complexity and temporal plasticity in pancreatic β-cells. *J Biosci* 25: 197–209, 2000.

7. **Bertram R, Sherman A, Kinard TA, and Satin LS.** The phantom bursting model for pancreatic β-cells. *Biophys J* 79: 2880–2892, 2000.
8. **Bertram R, Smolen P, Sherman A, Mears D, Atwater I, Martin F, and Soria B.** A role for calcium release-activated current (CRAC) in cholinergic modulation of electrical activity in pancreatic β-cells. *Biophys J* 68: 2323–2332, 1995.
9. **Bokvist K, Ammala C, Berggren PO, Rorsman P, and Wahlander K.** Alpha 2-adrenoreceptor stimulation does not inhibit L-type calcium channels in mouse pancreatic β-cells. *Biosci Rep* 11: 147–157, 1991.
10. **Carafoli E.** The Ca^{2+} pump of the plasma membrane. *J Biol Chem* 267: 2115–2118, 1992.
11. **Carignani C, Roncarati R, Rimini R, and Terstappen GC.** Pharmacological and molecular characterisation of SK3 channels in the TE671 human medulloblastoma cell line. *Brain Res* 939: 11–18, 2002.
12. **Chapman JB, Johnson EA, and Kootsey JM.** Electrical and biochemical properties of an enzyme model of the sodium pump. *J Membr Biol* 74: 139–153, 1983.
13. **Chay TR.** Electrical bursting and luminal calcium oscillation in excitable cell models. *Biol Cybern* 75: 419–443, 1996.
14. **Chay TR.** Effects of extracellular calcium on electrical bursting and intracellular and luminal calcium oscillations in insulin secreting pancreatic β-cells. *Biophys J* 73: 1673–1688, 1997.
15. *Content*. Amsterdam, The Netherlands: Centrum voor Wiskunde en Informatica. [online] ftp://ftp.cwi.nl/pub/CONTENT
16. **Dean PM.** Ultrastructural morphometry of the pancreatic β-cell. *Diabetologia* 9: 115–119, 1973.
17. **Deeney JT, Kohler M, Kubik K, Brown G, Schultz V, Tornheim K, Corkey BE, and Berggren PO.** Glucose-induced metabolic oscillations parallel those of Ca^{2+} and insulin release in clonal insulin-secreting cells. A multiwell approach to oscillatory cell behavior. *J Biol Chem* 276: 36946–36950, 2001.
18. **Deeney JT, Prentki M, and Corkey BE.** Metabolic control of β-cell function. *Semin Cell Dev Biol* 11: 267–275, 2000.
19. **Detimary P, Gilon P, and Henquin JC.** Interplay between cytoplasmic Ca^{2+} and the ATP/ADP ratio: a feedback control mechanism in mouse pancreatic islets. *Biochem J* 333: 269–274, 1998.
20. **DiPolo R and Beauge L.** Ionic ligand interactions with the intracellular loop of the sodium-calcium exchanger. Modulation by ATP. *Prog Biophys Mol Biol* 80: 43–67, 2002.
21. **Eberhardson M and Grapengiesser E.** Glucose and tolbutamide trigger transients of Ca^{2+} in single pancreatic β-cells exposed to tetraethylammonium. *Cell Calcium* 25: 355–360, 1999.
22. **Eberhardson M, Patterson S, and Grapengiesser E.** Microfluorometric analysis of Cl^- permeability and its relation to oscillatory Ca^{2+} signalling in glucose-stimulated pancreatic β-cells. *Cell Signal* 12: 781–786, 2000.
23. **Erecinska M, Bryla J, Michalik M, Meglasson MD, and Nelson D.** Energy metabolism in islets of Langerhans. *Biochim Biophys Acta* 1101: 273–295, 1992.
24. **Fatherazi S and Cook DL.** Specificity of tetraethylammonium and quinine for three K channels in insulin-secreting cells. *J Membr Biol* 120: 105–114, 1991.
25. **Gall D, Gromada J, Susa I, Rorsman P, Herchuelz A, and Bokvist K.** Significance of Na/Ca exchange for Ca^{2+} buffering and electrical activity in mouse pancreatic β-cells. *Biophys J* 76: 2018–2028, 1999.
26. **Gall D and Susa I.** Effect of Na/Ca exchange on plateau fraction and $[Ca]_i$ in models for bursting in pancreatic β-cells. *Biophys J* 77: 45–53, 1999.
27. **Gilon P, Arredouani A, Gailly P, Gromada J, and Henquin JC.** Uptake and release of Ca^{2+} by the endoplasmic reticulum contribute to the oscillations of the cytosolic Ca^{2+} concentration triggered by Ca^{2+} influx in the electrically excitable pancreatic β-cell. *J Biol Chem* 274: 20197–20205, 1999.
28. **Gilon P, Ravier MA, Jonas JC, and Henquin JC.** Control mechanisms of the oscillations of insulin secretion in vitro and in vivo. *Diabetes* 51: S144–S151, 2002.
29. **Gilon P, Yakel J, Gromada J, Zhu Y, Henquin JC, and Rorsman P.** G protein-dependent inhibition of L-type Ca^{2+} currents by acetylcholine in mouse pancreatic β-cells. *J Physiol* 499: 65–76, 1997.
30. **Giugliano M, Bove M, and Grattarola M.** Insulin release at the molecular level: metabolic-electrophysiological modeling of the pancreatic β-cells. *IEEE Trans Biomed Eng* 47: 611–623, 2000.
31. **Goforth PB, Bertram R, Khan FA, Zhang M, Sherman A, and Satin LS.** Calcium-activated K(+) channels of mouse beta-cells are controlled by both store and cytoplasmic Ca(2+): experimental and theoretical studies. *J Gen Physiol* 20: 307–322, 2002.
32. **Göpel SO, Kanno T, Barg S, Eliasson L, Galvanovskis J, Renstrom E, and Rorsman P.** Activation of Ca^{2+}-dependent K^+ channels contributes to rhythmic firing of action potentials in mouse pancreatic β-cells. *J Gen Physiol* 114: 759–770, 1999.
33. **Göpel SO, Kanno T, Barg S, Galvanovskis J, and Rorsman P.** Voltage-gated and resting membrane currents recorded from β-cells in intact mouse pancreatic islets. *J Physiol* 521: 717–728, 1999.
34. **Grapengiesser E.** Glucose induces cytoplasmic Na^+ oscillations in pancreatic beta-cells. *Biochem Biophys Res Commun* 226: 830–835, 1996.
35. **Grapengiesser E.** Unmasking of a periodic Na^+ entry in glucose-stimulated pancreatic β-cells after partial inhibition of the Na/K pump. *Endocrinology* 139: 3227–3231, 1998.
36. **Gromada J, Frokjaer-Jensen J, and Dissing S.** Glucose stimulates voltage- and calcium-dependent inositol trisphosphate production and intracellular calcium mobilization in insulin-secreting in βTC3 cells. *Biochem J* 314: 339–345, 1996.
37. **Gylfe E, Ahmed M, Bergsten P, Dansk H, Dyachok O, Eberhardson M, Grapengiesser E, Hellman B, Lin JM, Sundsten T, Tengholm A, Vieira E, and Westerlund J.** Signaling underlying pulsatile insulin secretion. *Ups J Med Sci* 105: 35–51, 2000.
38. **Hagar RE and Ehrlich BE.** Regulation of the type III $InsP_3$ receptor and its role in β-cell function. *Cell Mol Life Sci* 57: 1938–1949, 2000.
39. **Hagar RE and Ehrlich BE.** Regulation of the type III InsP(3) receptor by InsP(3) and ATP. *Biophys J* 79: 271–278, 2000.
40. **Hao L, Rigaud JL, and Inesi G.** Ca^{2+}/H^+ countertransport and electrogenicity in proteoliposomes containing erythrocyte plasma membrane Ca-ATPase and exogenous lipids. *J Biol Chem* 269: 14268–14275, 1994.
41. **Hille B.** *Ion Channels and Excitable Membranes* (3rd ed.). Sunderland, MS: Sinauer Associated, 2001.
42. **Hirose K, Kadowaki S, Tanabe M, Takeshima H, and Iino M.** Spatiotemporal dynamics of inositol 1,4,5-trisphosphate that underlies complex Ca^{2+} mobilization patterns. *Science* 284: 1527–1530, 1999.
43. **Hopkins WF, Fatherazi S, Peter-Riesch B, Corkey BE, and Cook DL.** Two sites for adenine-nucleotide regulation of ATP-sensitive potassium channels in mouse pancreatic β-cells and HIT cells. *J Membr Biol* 129: 287–295, 1992.
44. **Kanno T, Rorsman P, and Göpel SO.** Glucose-dependent regulation of rhythmic action potential firing in pancreatic beta-cells by K(ATP)-channel modulation. *J Physiol* 545: 501–507, 2002.
45. **Kanno T, Suga S, Wu J, Kimura M, and Wakui M.** Intracellular cAMP potentiates voltage-dependent activation of L-type Ca^{2+} channels in rat islet β-cells. *Pflügers Arch* 435: 578–580, 1998.
46. **Keizer J and Magnus G.** ATP-sensitive potassium channel and bursting in the pancreatic β-cell. A theoretical study. *Biophys J* 56: 229–242, 1989.
47. **Kitasato H, Kai R, Ding WG, and Omatsu-Kanbe M.** The intrinsic rhythmicity of spike-burst generation in pancreatic β-cells and intercellular interaction within an islet. *Jpn J Physiol* 46: 363–373, 1996.
48. **Kinard TA, deVries D, Sherman A, and Satin LS.** Modulation of the bursting properties of single mouse pancreatic β-cells by artificial conductances. *Biophys J* 76: 1423–1435, 1999.
49. **Köhler M, Hirschberg B, Bond CT, Kinzie JM, Marrion NV, Maylie J, and Adelman JP.** Small-conductance, calcium-activated potassium channels from mammalian brain. *Science* 273: 1709–1714, 1996.
50. **Kukuljan M, Goncaves AG, and Atwater I.** Charybdotoxin-sensitive $K_{(Ca)}$ channel is not involved in glucose-induced electrical activity in pancreatic β-cells. *J Membr Biol* 119: 187–195, 1991.

51. **Larsson O, Kindmark H, Bränström R, Fredholm B, and Berggren PO.** Oscillations in KATP channel activity promote oscillations in cytoplasmic free Ca^{2+} concentration in the pancreatic β-cell. *Proc Natl Acad Sci USA* 93: 5161–5165, 1996.
52. **Leech CA and Habener JF.** A role for Ca^{2+} sensitive nonselective cation channels in regulating the membrane potential of pancreatic β-cells. *Diabetes* 47: 1066–1073, 1998.
53. **Leinders T and Vijverberg HPM.** Ca^{2+} dependence of small Ca^{2+}-activated K^+ channels in cultured N1E-115 mouse neuroblastoma cells. *Pflügers Arch* 422: 223–232, 1992.
54. **Liu YJ, Tengholm A, Grapengiesser E, Hellman B, and Gylfe E.** Origin of slow and fast oscillations of Ca^{2+} in mouse pancreatic islets. *J Physiol* 508: 471–481, 1998.
55. **Loew LM and Schaff JC.** The virtual cell: a software environment for computational cell biology. *Trends Biotechnol* 19: 401–406, 2001.
56. **MacDonald PE, Ha XF, Wang J, Smukler SR, Sun AM, Gaisano HY, Salapatek AM, Backx PH, and Wheeler MB.** Members of the Kv1 and Kv2 voltage-dependent K^+ channel families regulate insulin secretion. *Mol Endocrinol* 15: 1423–1435, 2001.
57. **Maes K, Missiaen L, De Smet P, Vanlingen S, Callewaert G, Parys JB, and De Smedt H.** Differential modulation of inositol 1,4,5-trisphosphate receptor type 1 and type 3 by ATP. *Cell Calcium* 7: 257–267, 2000.
58. **Magnus G and Keizer J.** Model of β-cell mitochondrial calcium handling and electrical activity. I. Cytoplasmic variables. *Am J Physiol Cell Physiol* 274: C1158–C1173, 1998.
59. **Magnus G and Keizer J.** Model of β-cell mitochondrial calcium handling and electrical activity. II. Mitochondrial variables. *Am J Physiol Cell Physiol* 274: C1174–C1184, 1998.
60. **Mak DO, McBride S, and Foskett JK.** Regulation by Ca^{2+} and inositol 1,4,5-trisphosphate (InsP3) of single recombinant type 3 InsP3 receptor channels. Ca^{2+} activation uniquely distinguishes types 1 and 3 insp3 receptors. *J Gen Physiol* 117: 435–446, 2001.
61. **Matschinsky FM, Landgraf R, Ellerman J, and Kotler-Brajtburg J.** Glucoreceptor mechanisms in islets of Langerhans. *Diabetes* 21, *Suppl* 2: 555–569, 1972.
62. **Mears D, Sheppard NF Jr, Atwater I, Rojas E, Bertram R, and Sherman A.** Evidence that calcium release-activated current mediates transient glucose-induced electrical activity in the pancreatic β-cell. *J Membr Biol* 155: 47–55, 1997.
63. **Meyer T, Wensel T, and Stryer L.** Kinetics of calcium channel opening by inositol 1,4,5-trisphosphate. *Biochemistry* 29: 32–37, 1990.
64. **Miura Y, Henquin JC, and Gilon P.** Emptying of intracellular Ca^{2+} stores stimulates Ca^{2+} entry in mouse pancreatic beta-cells by both direct and indirect mechanisms. *J Physiol* 503: 387–398, 1997.
65. **Miwa Y and Imai Y.** Simulation of spike-burst generation and Ca^{2+} oscillation in pancreatic β-cells. *Jpn J Physiol* 49: 353–364, 1999.
66. **Moller JV, Juul B, and le Maire M.** Structural organization, ion transport, and energy transduction of P-type ATPases. *Biochim Biophys Acta* 1286: 1–51, 1996.
67. **Nygren A, Fiset C, Firek L, Clark JW, Lindblad DS, Clark RB, and Giles WR.** Mathematical model of an adult human atrial cell: the role of K^+ currents in repolarization. *Circ Res* 82: 63–81, 1998.
68. **Owada S, Larsson O, Arkhammar P, Katz AI, Chibalin AV, Berggren PO, and Bertorello AM.** Glucose decreases Na^+,K^+-ATPase activity in pancreatic β-cells. An effect mediated via Ca^{2+}-independent phospholipase A2 and protein kinase C-dependent phosphorylation of the alpha-subunit. *J Biol Chem* 274: 2000–2008, 1999.
69. **Petersen OH, Tepikin A, and Park MK.** The endoplasmic reticulum: one continuous or several separate Ca^{2+} stores? *Trends Neurosci* 24: 271–276, 2001.
70. **Philipson LH.** β-Cell ion channels: keys to endodermal excitability. *Horm Metab Res* 31: 455–461, 1999.
71. **Rice JJ, Jafri MS, and Winslow RL.** Modeling short-term interval-force relations in cardiac muscle. *Am J Physiol Heart Circ Physiol* 278: H913–H931, 2000.
72. **Roe MW, Lancaster ME, Mertz RJ, Worley JF III, and Dukes ID.** Voltage-dependent intracellular calcium release from mouse islets stimulated by glucose. *J Biol Chem* 268: 9953–9956, 1993.
73. **Roe MW, Worley JF III, Mittal AA, Kuznetsov A, DasGupta S, Mertz RJ, Witherspoon SM III, Blair N, Lancaster ME, McIntyre MS, Shehee WR, Dukes ID, and Philipson LH.** Expression and function of pancreatic β-cell delayed rectifier K^+ channels. Role in stimulus-secretion coupling. *J Biol Chem* 271: 32241–32246, 1996.
74. **Roe MW, Worley JF III, Qian F, Tamarina N, Mittal AA, Dralyuk F, Blair NT, Mertz RJ, Philipson LH, and Dukes ID.** Characterization of a Ca^{2+} release-activated nonselective cation current regulating membrane potential and $[Ca^{2+}]_i$ oscillations in transgenically derived β-cells. *J Biol Chem* 273: 10402–10410, 1998.
75. **Rosario LM, Barbosa RM, Antunes CM, Silva AM, Abrunhosa AJ, and Santos RM.** Bursting electrical activity in pancreatic β-cells: evidence that the channel underlying the burst is sensitive to Ca^{2+} influx through L-type Ca^{2+} channels. *Pflügers Arch* 424: 439–447, 1993.
76. **Rorsman P.** The pancreatic β-cell as a fuel sensor: an electrophysiologist's viewpoint. *Diabetologia* 40: 487–495, 1997.
77. **Rorsman P, Ammala C, Berggren PO, Bokvist K, and Larsson O.** Cytoplasmic calcium transients due to single action potentials and voltage-clamp depolarizations in mouse pancreatic β-cells. *EMBO J* 11: 2877–2884, 1992.
78. **Sherman A.** Contributions of modeling to understanding stimulus-secretion coupling in pancreatic β-cells. *Am J Physiol Endocrinol Metab* 271: E362–E372, 1996.
79. **Sims CE and Allbritton NL.** Metabolism of inositol 1,4,5-trisphosphate and inositol 1,3,4,5-tetrakisphosphate by the oocytes of *Xenopus laevis*. *J Biol Chem* 273: 4052–4058, 1998.
80. **Smith PA, Aschroft FM, and Fewtrell CM.** Permeation and gating properties of the L-type calcium channel in mouse pancreatic β-cells. *J Gen Physiol* 101: 767–797, 1993.
81. **Smith PA, Ashcroft FM, and Rorsman P.** Simultaneous recordings of glucose dependent electrical activity and ATP-regulated K^+-currents in isolated mouse pancreatic β-cells. *FEBS Lett* 261: 187–190, 1990.
82. **Smolen P and Keizer J.** Slow voltage inactivation of Ca^{2+} currents and bursting mechanisms for the mouse pancreatic β-cell. *J Membr Biol* 127: 9–19, 1992.
83. **Soria B and Martin F.** Cytosolic calcium oscillations and insulin release in pancreatic islets of Langerhans. *Diabetes Metab* 24: 37–40, 1998.
84. **Straub SG, Kornreich B, Oswald RE, Nemeth EF, and Sharp GW.** The calcimimetic R-467 potentiates insulin secretion in pancreatic β-cells by activation of a nonspecific cation channel. *J Biol Chem* 275: 18777–18784, 2000.
85. **Sturis J, Pugh WL, Tang J, Ostrega DM, Polonsky JS, and Polonsky KS.** Alterations in pulsatile insulin secretion in the Zucker diabetic fatty rat. *Am J Physiol Endocrinol Metab* 267: E250–E259, 1994.
86. **Tengholm A, Hellman B, and Gylfe E.** The endoplasmic reticulum is a glucose-modulated high-affinity sink for Ca^{2+} in mouse pancreatic β-cells. *J Physiol* 530: 533–540, 2001.
87. **Varadi A, Molnar E, and Ashcroft SJ.** Characterisation of endoplasmic reticulum and plasma membrane Ca^{2+}-ATPases in pancreatic β-cells and in islets of Langerhans. *Biochim Biophys Acta* 1236: 119–127, 1995.
88. **Worley JK III, McIntyre MS, Spencer B, and Dukes ID.** Depletion of intracellular Ca^{2+} stores activates a maitotoxin-sensitive nonselective cationic current in β-cells. *J Biol Chem* 269: 32055–32058, 1994.
89. **Worley JF III, McIntyre MS, Spencer B, Mertz RJ, Roe MW, and Dukes ID.** Endoplasmic reticulum calcium store regulates membrane potential in mouse islet β-cells. *J Biol Chem* 269: 14359–14362, 1994.